For Reference

NOT TO BE TAKEN FROM THIS ROOM

For Reference

NOT TO BE TAKEN FROM THIS ROOM

Ex libris
Universitatis
Albertaensis

UNIVERSITY OF ALBERTA
QUAECUMQUE VERA

University of Alberta
Printing Department

Thesis
1960(F)
#8

THE UNIVERSITY OF ALBERTA

THE EFFECT OF A MAGNETIC FIELD ON SOLIDIFICATION MECHANISMS

A THESIS
SUBMITTED TO THE FACULTY OF GRADUATE STUDIES
IN PARTIAL FULFILMENT OF THE REQUIREMENTS FOR THE DEGREE
OF MASTER OF SCIENCE

DEPARTMENT OF MINING AND METALLURGY

by

DOUGLAS ROY COLTON

EDMONTON, ALBERTA
SEPTEMBER, 1960

UNIVERSITY OF ALBERTA

FACULTY OF GRADUATE STUDIES

The undersigned certify that they have read, and recommend to the Faculty of Graduate Studies for acceptance, a thesis entitled

THE EFFECT OF A MAGNETIC FIELD
ON SOLIDIFICATION MECHANISMS

submitted by DOUGLAS ROY COLTON

in partial fulfilment of the requirements for the degree of Master of Science.

ABSTRACT:

The effect of a magnetic field on the solidification of binary alloys of bismuth with antimony and tin was studied using the maximum segregation at the base of the unidirectionally solidified ingots as a criterion. The segregation in the "magnetically" solidified ingots was found to be appreciably different from the segregation in the normally solidified ingots. The equations of the theory of inverse segregation were used to calculate theoretical segregation values for the normally solidified ingots. For the bismuth-antimony system the calculated and experimental segregation values for the normally cast ingots were in good quantitative agreement. The results for the bismuth-tin system were only qualitatively in agreement. The "magnetically" cast and the normally cast ingots showed morphological differences which were most distinct in the bismuth-rich bismuth-tin alloys.

Digitized by the Internet Archive
in 2019 with funding from
University of Alberta Libraries

https://archive.org/details/effectofmagnetic00doug_0

ACKNOWLEDGEMENTS

The author wishes to express his gratitude to Dr. W. V. Youdelis whose inspiration and guidance during his direction of this project has been invaluable. He is also indebted to Dr. J. Gordon Parr for his many helpful criticisms and suggestions and to Professor E. O. Lilge for his sympathetic and helpful departmental supervision.

The donation of the metals used in this project by The Consolidated Mining and Smelting Company of Canada Limited is gratefully acknowledged. Finally, the author is particularly grateful to the National Research Council who furnished the grant which made the project possible.

TABLE OF CONTENTS

Page

INTRODUCTION 1

HISTORICAL REVIEW 2

THEORY
- A. Solidification Theory 4
  - (1) Nucleation and Growth 4
  - (2) Preferred Growth Directions and Columnar Crystals 4
  - (3) Dendritic Growth 5
  - (4) Equiaxial Crystals 7
  - (5) Segregation 8
- B. Magnetic Theory 10
  - (1) Ferromagnetism 10
  - (2) Paramagnetism
  - (3) Diamagnetism 12
- C. The Alloying Properties of Bismuth with Antimony and Tin 13
- D. The Magnetic Properties of the Alloys of Bismuth with Antimony and Tin 14

EXPERIMENTAL
- (1) Apparatus 17
- (2) Method 23

RESULT
- (1) Metallographic 24
- (2) Segregation 25

DISCUSSION
- A. The System Bi-Sb 43
  - (1) Crystal Morphology 43
  - (2) Segregation 44
- B. The System Bi-Sn 47
  - (1) Crystal Morphology 47
  - (2) Segregation 50

SUMMARY AND CONCLUSIONS 51

Page

BIBLIOGRAPHY 52

APPENDIX I - Calculation of the Segregation 54

APPENDIX II - Construction of the Solenoid 60

APPENDIX III - Methods of Analysis 67

FIGURES AND ILLUSTRATIONS

Page

1. Equilibrium Liquidus and Specimen Temperature ahead of an Advancing Plane Interface of a Binary Alloy. 6

2. The Diamagnetic Susceptibility of the Alloys of Bismuth with Antimony and with Tin 15

3. The Influence of Temperature Upon the Magnetic Susceptibility of Bismuth Alloys 16

4. Photograph of the Apparatus Assembly 18

5. Photograph of the Casting Unit and Furnace 19

6. Diagram of the Casting Unit 20

7. Oscilloscope Trace of the Direct Current Output of a Rectifier-Type Welding Generator 22

8. Macrostructure of a Normally Cast 15% Bi-Sb Ingot .... x 1 1/2 26

9. Macrostructure of a Field Cast 15% Bi-Sb Ingot .... x 1 1/2 26

10. Macrostructure of a Normally Cast 70% Bi-Sb Ingot .... x 1 1/2 27

11. Macrostructure of a Field Cast 70% Bi-Sb Ingot .... x 1 1/2 27

12. Microstructure of the Base of a Normally Cast 70% Bi-Sb Ingot .... x 100 28

12a. Microstructure of the Normally Cast 70% Bi-Sb Ingot .... x 600 28A

13. Microstructure of the Base of a Field Cast 70% Bi-Sb Ingot .... x 100 28

13a. Microstructure of the Field Cast 70% Bi-Sb Ingot .... x 600 28A

14. Macrostructure of a Normally Cast 15% Bi-Sn Ingot .... x 1 1/2 29

Page

15. Macrostructure of a Field Cast 15% Bi-Sn Ingot .... x 1 1/2 29

16. Macrostructure of a Normally Cast 60% Bi-Sn Ingot .... x 1 1/2 30

17. Macrostructure of a Field Cast 60% Bi-Sn Ingot .... x 1 1/2 30

18. Macrostructure of a Normally Cast 70% Bi-Sn Ingot .... x 1 1/2 31

19. Macrostructure of a Field Cast 70% Bi-Sn Ingot .... x 1 1/2 31

20. Macrostructure of a Normally Cast 80% Bi-Sn Ingot .... x 1 1/2 32

21. Macrostructure of a Field Cast 80% Bi-Sn Ingot .... x 1 1/2 32

22. Macrostructure of a Normally Cast 85% Bi-Sn Ingot .... x 1 1/2 33

23. Macrostructure of a Field Cast 85% Bi-Sn Ingot .... x 1 1/2 33

24. Macrostructure of a Normally Cast 90% Bi-Sn Ingot .... x 1 1/2 34

25. Macrostructure of a Field Cast 90% Bi-Sn Ingot .... x 1 1/2 34

26. Macrostructure of the Base of a Normally Cast 85% Bi-Sn Ingot Showing Dendritic Growth ... x 20 35

27. Macrostructure of the Base of a Field Cast 85% Bi-Sn Ingot Showing Partial Destruction of the Dendrites by the Field .... x 20 35

28. Macrostructure of the Equiaxial Crystals Occurring at the Center of a Normally Cast 85% Bi-Sn Ingot .... x 20 36

Page

29. Macrostructure of the Equiaxial Crystals Occurring at the Center of a Field Cast 85% Bi-Sn Ingot Showing Orientation by the Field .... x 20 36

30. Microstructure of the Base of a Normally Cast 85% Bi-Sn Ingot .... x 100 37

31. Microstructure of the Base of a Field Cast 85% Bi-Sn Ingot .... x 100 37

32. Cooling Curves for Bi-Sb Alloys 38

33. Cooling Curves for Bi-Sn Alloys 39

34. Theoretical and Experimental Segregation Curves for the System Bi-Sb 40

35. Theoretical and Experimental Segregation Curves for the System Bi-Sn 41

36. Normal and "Field" Equilibrium Diagrams for the System Bi-Sb 42

37. Orientation of a Bismuth Crystal by a Magnetic Field Compared to the Direction of Highest Thermal Conductivity 49A

38. Equilibrium Diagram and Specific Volume Data for the System Bi-Sb 58

39. Equilibrium Diagram and Specific Volume Data for the System Bi-Sn 59

40. Cross Section of the Solenoid 65

41. Schematic Illustration of the Solenoid Mounting and Controls. 66

INTRODUCTION

The solidification mechanisms of an alloy sample are well known to be directly related to the equilibrium phase relationships of the alloy. Thus one may interpret the phenomena of dendritic growth and of coring by referring to the equilibrium phase diagram for the alloy system. In turn, the phase relationships of the alloy system are directly related to the electronic structure of the component atoms as has been demonstrated by Hume-Rothery(1). Further, the electronic structure of an alloy may be influenced by the application of a magnetic field. Evidence for this is given by the phenomena of magnetic susceptibility, the change in electrical and thermal conductivity of an alloy sample placed in a magnetic field, and the Hall effect. Finally, one is led, through consideration of the above facts, to the hypothesis that it might be possible to influence the solidification mechanisms of an alloy by the application of a magnetic field.

The principal criterion which was selected to analyse the effect of the field was the maximum segregation occurring at the base of a unidirectionally solidified ingot. The main reason for the selection was that this phenomenon gives rise to an effect that is measurable by the methods of ordinary chemical analysis and directly related in a quantitative manner to the phase diagram of the alloy

system. Thus a change in the boundaries of the phase fields would be quantitatively revealed by the change in segregation. An outline of segregation theory is given in Appendix I. The other criterion used to analyse the effect of the field was a comparison of the crystal morphology of the alloys solidified in the field with that of the normally solidified alloys.

The alloy systems selected for this investigation were those of bismuth with antimony and tin. The magnetic properties of bismuth have been extensively studied and the alloys formed by it with antimony and tin form systems suitable for study by the segregation method.

HISTORICAL REVIEW

A search of the literature did not reveal any experiments which dealt directly with the effect of a magnetic field on the solidification mechanisms of an alloy system. Much work has been done, however, which is closely related to the problem. The annealing of alloys of ferromagnetic material has been extensively studied by Bozorth(2) and his co-workers. They have established that magnetic annealing of a ferromagnetic alloy near the Curie temperature may greatly increase the permeability, an effect attributed to ordering. Klemm and Mayr(3) studied the effect of a magnetic field on the tempering

of a cobalt-copper alloy and observed that the field slightly altered the composition at which the alloys became ferromagnetic.

Goetz, Focke, and Hergenrother(4)(5), in a series of experiments, solidified a single crystal of bismuth in a magnetic field and studied the properties of the "magnetic" crystal in comparison to those of a normal crystal. They observed a change of density of about 0.3% which was not associated with any change of lattice parameter. Goetz and Focke attributed the change in density to the presence of a mosaic structure caused by imperfections.

Goetz and Focke(5) and also Shimizu(6) have established the anisotropic nature of the susceptibility of bismuth crystals and experiments have been made to determine the preferred orientation, if any, of crystals solidified in a field. Goetz did not find any orientation influence on a single crystal of bismuth grown from a seed crystal. On the other hand, Mayr(3), working with polycrystalline material, did find the field influenced the orientation of the crystals on solidification such that the trigonal axis was parallel to the field. The orientation noted by Mayr is in agreement with the work of Alma(7) on powdered bismuth crystals.

Nakagawa(8) has studied the change of susceptibility of transition metals upon melting and solidifying. An incidental observation made in the course of this work was the presence of a very large supercooling effect, amounting to several hundred degrees in some cases.

THEORY

In the following, a brief resume will be given of the theories of the solidification mechanisms and of the magnetic properties of metal alloys. This will be followed by a summary of the alloying and magnetic properties of the metals used in this experiment.

A. Solidification Theory

(1) Nucleation and Growth

The fundamental mechanisms of crystal growth have not been completely established. The two-dimensional nucleation theory, in which new atomic planes are formed by the growth of atom clusters deposited on the completed crystal faces, is useful in explaining crystal growth under conditions of supercooling and supersaturation but fails to explain the fast rate of growth under conditions of low supersaturation. Frank (11, 12) and his co-workers propose that dislocations in a crystal provide continuous re-entrant steps (spirals) which are low energy sites from which new atom planes grow.

(2) Preferred Growth Directions and Columnar Crystals

The preferred growth direction of crystals can be attributed to the higher forward rate of propagation of certain crystal faces as has been demonstrated by Chalmers(14, 15). The faster growth rate of

a preferred face (usually the less-closely packed planes of a crystal) results in a stepped interface at the boundary of two growing crystals. Growth onto the edge causes the boundary to diverge during growth crowding out the crystal that has its preferred direction of growth farthest from the direction of heat flow. This description qualitatively accounts for the columnar zone in ingots.

(3) Dendritic Growth

Tiller(16) et al have pointed out that during solidification of an alloy under fast cooling conditions, the finite diffusion rate of the solute in the liquid (of the order of 1-10 cm^2/day) will result in a pileup of the solute atoms at the solid-liquid interface. Further development of this concept by Rutter and Chalmers(17) is embodied in their theory of "constitutional supercooling".

At the interface, where the solute concentration has increased, either the concentration or the temperature must fall if solidification is to proceed. Since the diffusion of atoms is usually very slow compared to the conduction of heat an increase of solute content at the interface will be accompanied by a decrease in interface temperature. The actual temperature will be below the equilibrium liquidus temperature whose form is determined by the distribution of the solute at the interface as shown by Figure 1. The liquid in the region between the interface and the point where the temperature curves

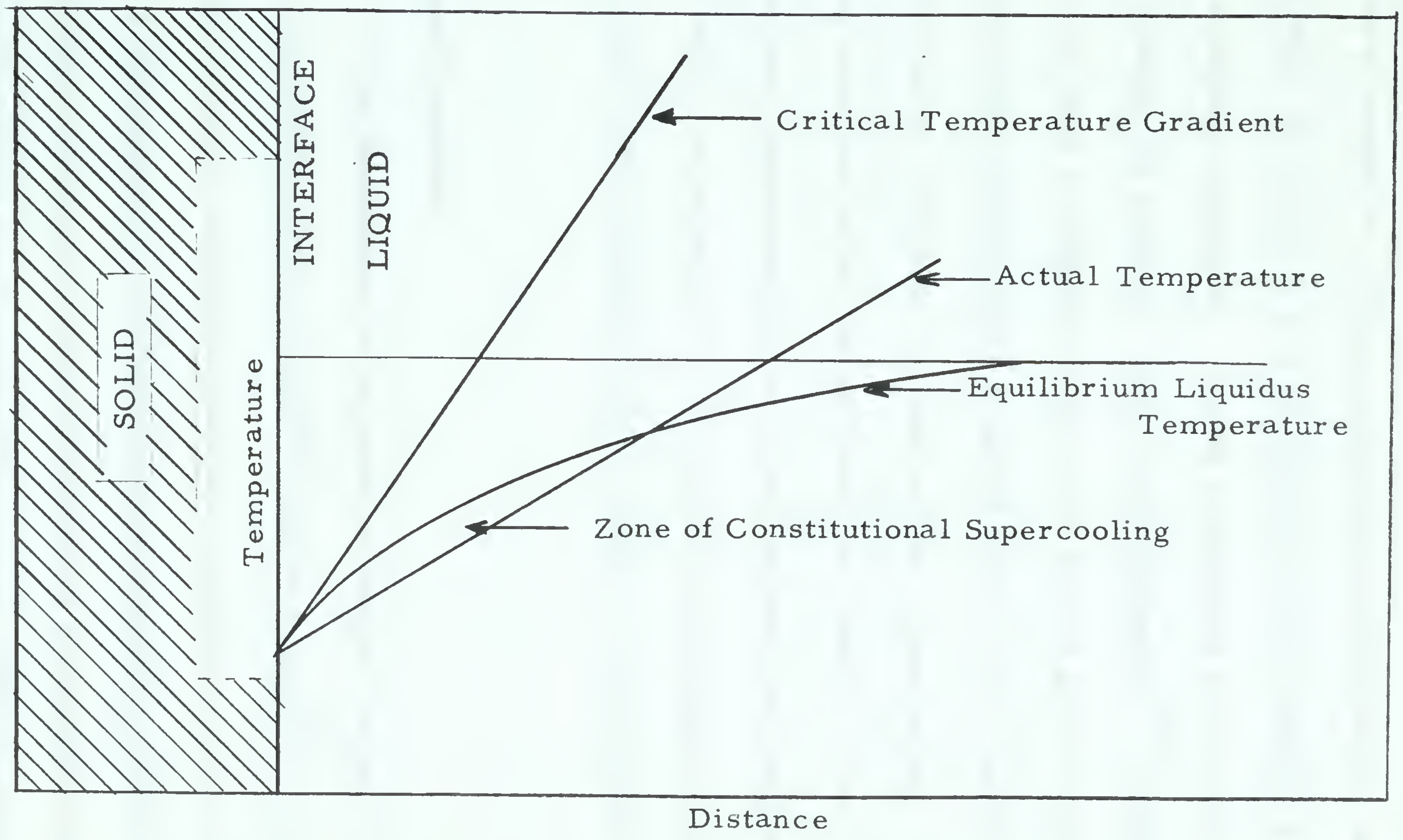
SOLID
Temperature
INTERFACE
LIQUID
Critical Temperature Gradient
Actual Temperature
Equilibrium Liquidus Temperature
Zone of Constitutional Supercooling
Distance

Fig. 1 Equilibrium Liquidus and Specimen Temperature Ahead of an Advancing Plane Interface of a Binary Alloy

intersect is therefore supercooled. Under these conditions it is possible for a crystal to initiate spontaneous solidification, without heat extraction, in the form of a projection at the interface giving the interface a cellular structure. These projections are the first manifestation of dendritic growth. Rutter and Chalmers (17) propose that the absence of such a cellular structure at slower growth speeds is due to the more uniform distribution of solute atoms in the liquid by diffusion thus destroying the condition of constitutional supercooling. Extremely fast cooling rates may also prevent dendritic growth by the elimination of constitutional supercooling, for if the temperature gradient is increased until it is tangential to the equilibrium liquidus temperature (Figure 1) close to the interface then no region of supercooled liquid remains.

(4) Equiaxial Crystals

The occurrence of equiaxial crystals in rapidly solidified ingots has been discussed by Ruddle(18) and by Cibula(19). They propose that the rise in solute concentration at an interface of a growing crystal results in a high degree of constitutional supercooling, which, if sufficiently high, will give rise to nucleation of crystallites ahead of the interface resulting in an equiaxial structure. With increased alloy content constitutional supercooling will increase, which in turn will increase the extent of equiaxial crystallization (as observed by Cibula).

(5) Segregation

The amount and composition of the phases present during the solidification of a binary alloy are indicated by the constitutional diagram, provided that freezing is slow enough to allow the distribution of the solute atoms in the liquid and in the solid phases to be made uniform by diffusion. However, during chill casting, solidification proceeds at a rate which precludes concentration equalization in the solid phase and may also limit it to the liquid. This redistribution of the solute at fast cooling rates is the primary mechanism which leads to inverse segregation in ingots.

Under conditions of near-equilibrium cooling the concentration gradients in the liquid and solid phases are eliminated by the process of diffusion and solidification will proceed by the slow advancement of a sharply delineated solid-liquid interface. This results in "normal" segregation in which the concentration of the component that lowers the melting point of the alloy is highest in regions of the ingot that solidify last.

Under normal, non-equilibrium conditions of solidification the phenomenon of inverse segregation is apt to occur. This is defined as the form of segregation in which the low melting point components which solidify last are found at greater than equilibrium concentration in the region of initial solidification, i.e., next to the chill face. The basic mechanism involved is solidification shrinkage upon formation

of the primary dendrites followed by interdendritic flow of the enriched residual liquid to compensate for the volume shrinkage. The drawing forces are related to the cohesive properties of the liquid.

A full description of the qualitative aspects of inverse segregation theory has been given by Adams(20). Scheil(21) formulated quantitative expressions for the amount of segregation occurring at the chill face for the alloys of a binary eutectic system. Scheil's formulae were redeveloped by Kirkaldy and Youdelis(22) and extended to include the degree of segregation throughout the length of a unidirectionally solidified ingot. The theory can also be applied to systems other than binary eutectic. Experimental verification has been established by Scheil and by Kirkaldy and Youdelis for the aluminum-copper system and by Youdelis and Colton(23) for the aluminum-zinc system.

The principal assumptions and equations of the quantitative theory of inverse segregation are given in Appendix I. It will be noted that the degree of segregation is a function of the constant "A" which is related to the slopes of the solidus and liquidus lines of the alloy system and which occurs as an exponent in the mass equations. Thus a segregation determination is a very sensitive means by which induced changes in solid solubility may be determined. It has also been shown that the maximum inverse segregation occurring at the chill face is independent of crystal morphology(9). The occurrence of an exudation of enriched liquid on the surface of the ingot base will alter the degree of segregation and, if present, must be corrected for since exudations occur by a different mechanism.

B. Magnetic Theory

Most metals fall into three main classifications as to their magnetic properties: ferromagnetic, paramagnetic and diamagnetic.

(1) Ferromagnetic

A ferromagnetic material is believed to be spontaneously magnetized, the unmagnetized state of the material being explained by the uncorrelated direction of the spontaneously magnetized "domains". The application of an external field aligns the domains through rotation or boundary migration resulting in a magnetic intensity many thousands of times greater than that of the applied field. Gyromagnetic experiments may be used to prove that the magnetization in ferromagnetics arises from the alignment of electron spin. In these experiments one measures the ratio of the magnetic moment to the angular momentum, either by reversing the magnetization of a suspended specimen and observing its rotation or by rotating the specimen and observing the magnetization. For an electron

$$\frac{\text{magnetic moment}}{\text{angular momentum}} = \frac{\frac{e\hbar}{2mc}}{\frac{\hbar}{mc}} = \frac{e}{mc}$$

where

m = mass of an electron
e = charge on an electron
$\hbar$ = Planck's constant divided by 2π
c = velocity of light

This is equated to the magnetomechanical factor, $\frac{g'e}{2mc}$,

where g' is the Lande g' factor, giving for electron spin g' = 2. The experimental values of g' for ferromagnetic materials are usually between 1.85 and 2.0, showing that the major contribution comes from electron spin.

(2) Paramagnetic

Paramagnetic substances are usually further divided into:

(a) Strongly paramagnetic substances having a susceptibility dependent upon the temperature. This is due to a nearly free magnetic core in the atom. It is exhibited by the strongly ionic rare earths and their salts.

(b) Weak spin paramagnetism which is approximately independent of the temperature. If the Bohr magneton, μ, is denoted by $\frac{e\hbar}{2mc}$, then in an external magnetic field H, the energy of an electron can take two values, $-H\mu$ if the spin points parallel to the field, or $+H\mu$ if the spin points antiparallel. An electron will tend to turn parallel to the field and transfer the energy $2H\mu$ to the lattice vibrations. Only for a few electrons of a metal, which are in excited states, are there unoccupied parallel states to which to turn. (A consequence of the Pauli exclusion principle). This gives rise to a small temperature independent paramagnetism. In the measurements of bulk susceptibility this paramagnetic susceptibility may be masked by the diamagnetism of the conduction electrons. As the diamagnetism disappears upon melting this gives rise to a small paramagnetic susceptibility of some

metals in the liquid state.

(3) Diamagnetism

The diamagnetism of the conduction electrons in metals arises from the translational motion of the electrons in a manner roughly in accord with Lenz's law. The rigorous calculation of the susceptibility involves the energy levels and the wave functions of the conduction electrons in a magnetic field as influenced by the periodic potential of the lattice. The problem is complex and has not been completely solved. The diamagnetic susceptibility of metals and alloys is usually given in terms of Brillouin zone theory. In this manner Jones(37) has explained the strong diamagnetism of bismuth and antimony. In these metals the electrons almost fill a Brillouin zone, with a small number of electrons overlapping into the next zone and an equal number of positive holes (unoccupied energy states in the k-space of the lower incompletely filled Brillouin zone). In the neighborhood of a small energy discontinuity at the zone boundary the effective mass of the electrons is very small (due to momentum transfer between the electron and the lattice when the wave propagation vector approaches the value for a Bragg reflection) and the electrons are very susceptible to the effect of this field. Also, those few electrons that overlap into the second zone have available energy states into which they may be excited by a magnetic field. In relation to this description, the Hall effect

forms an important concept. When a conductor is placed in a magnetic field perpendicular to the direction of current flow, a voltage is developed across the specimen in the direction perpendicular to both the current and the magnetic field. A positive Hall voltage implies that the current is carried by positive charges or holes. A negative Hall voltage implies that electrons are the carriers. The very large negative value of the voltage for bismuth is interpreted by band theory as being caused by a low concentration of electrons outside nearly filled bands or zones. The Hall voltage for bismuth is strongly influenced by the strength of the field and by alloying the bismuth with small amounts of tin.

C. The Alloying Properties of Bismuth with Antimony and with Tin.

The phase diagram for the bismuth system is given in Figure 38. Bismuth crystallizes in a rhombohedral structure in which the distance of closest approach of the atoms is 3.111 A^{o}. Antimony also crystallizes in a rhombohedral structure in which the distance of closest approach of the atoms is 2.903 A^{o}. Bismuth and antimony exhibit complete solid solubility.

The phase diagram for the bismuth-tin system is shown in Figure 39. The crystal structure of white tin might be described as a very distorted form of the diamond in which the distance of closest approach of the atoms is 3.111 A^{o}. Bismuth and tin exhibit limited solid

solubility with the formation of a eutectic. The exact solid solubility of tin in bismuth is not known. Values for the solubility have been inferred from X-ray measurements, susceptibility measurements, resistance measurements and many other forms of physical data but the results are inexact and anomalous. This subject is discussed in more detail in the interpretation of the experimental results.

D. The Magnetic Properties of Bismuth with Antimony and with Tin

The following data are reproduced from the work of Goetz and Focke(5), who have described at some length the nature of the crystal diamagnetism of bismuth and of its alloys with antimony and with tin. Of particular importance to this experiment are the relatively high susceptibilities of these alloys, the effect of temperature on the susceptibility, and the anisotropic nature of the susceptibility. Figure 2 gives the susceptibility variation with composition at room temperature. Figure 3 shows the variation of the susceptibility with temperature and, as separate values are given for directions normal to and parallel with the trigonal axis, it also illustrates the anisotropy.

Wolf and Goetz(24) have determined the magnetostriction of single crystals of bismuth, a factor which indicates the distortion of the lattice by the field. In fields of about ten kilogauss, comparable to

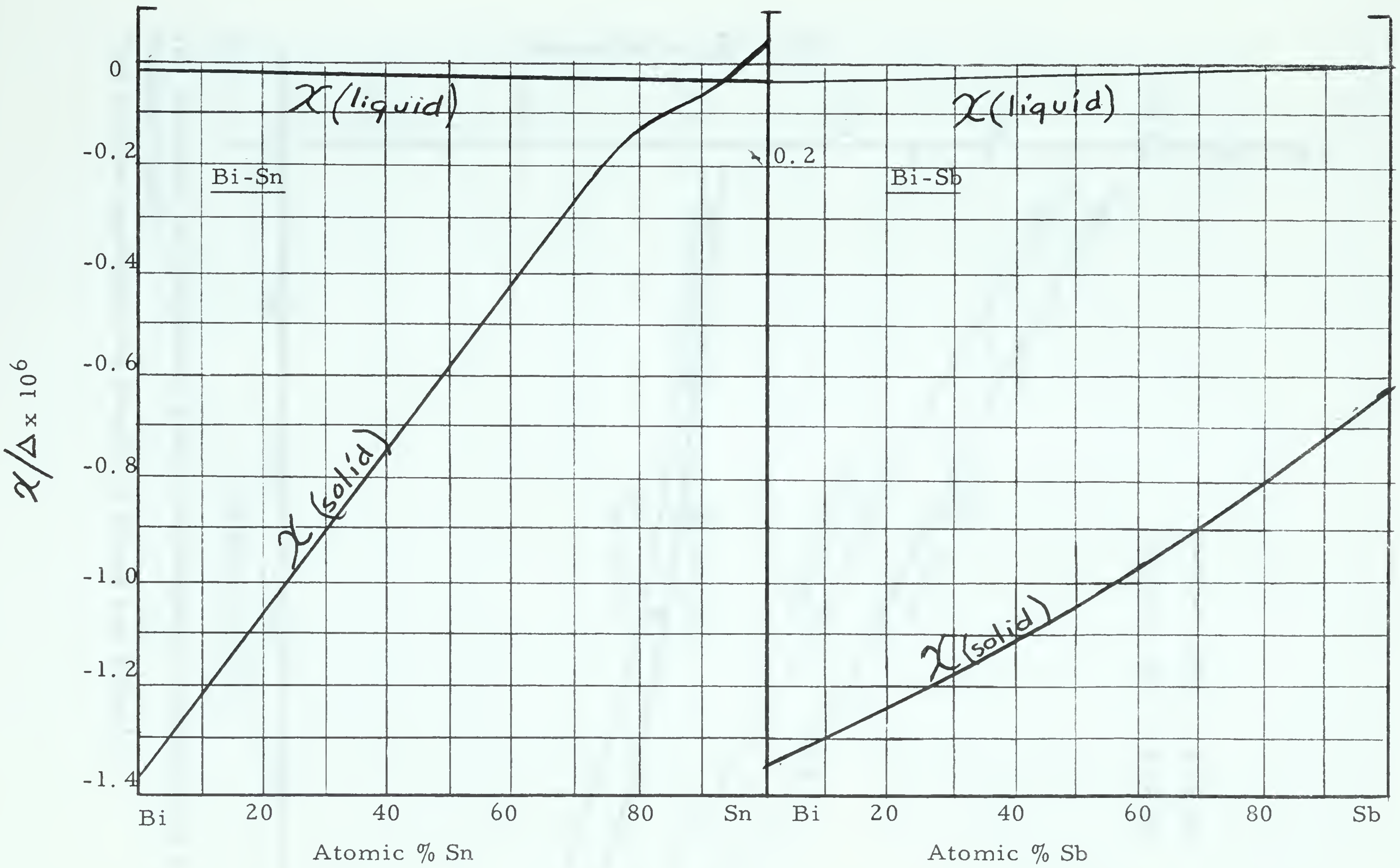

Fig. 2 The Magnetic Susceptibility of the Alloys of Bismuth with Antimony and with Tin (the curves represent the results of Shimizu[(6)])

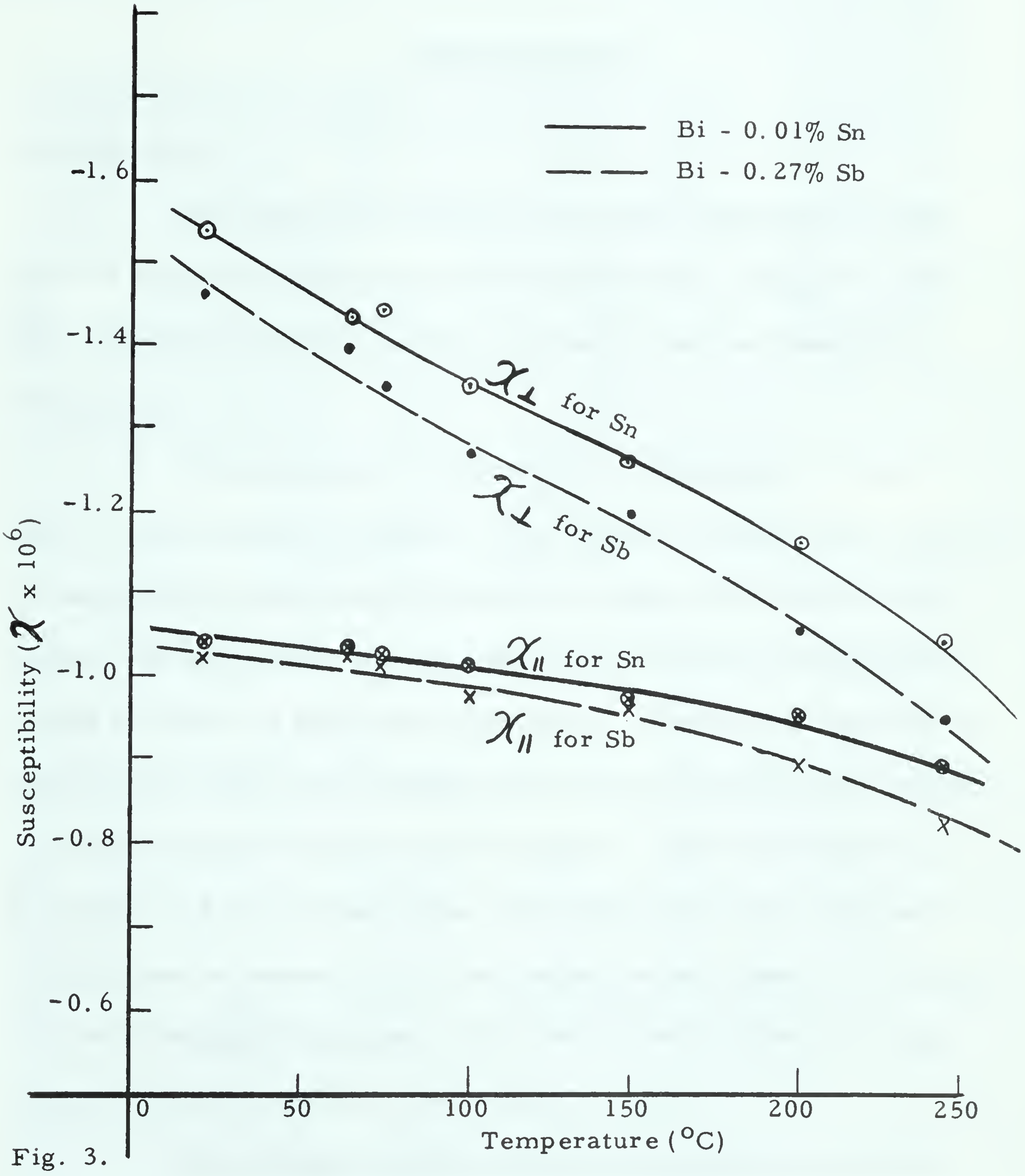

Fig. 3.

The Influence of Temperature upon the Magnetic Susceptibility of Bismuth Alloys.
The Curves represent the results of Goetz and Focke(5).

those used in this experiment, the value given for $\Delta l/l$ is only 1×10^{-6}, a value which indicates very little distortion by a field of that strength.

EXPERIMENTAL

(1) Apparatus

The apparatus consisted of a small casting unit around which a solenoid could be lowered to superimpose a magnetic field. The complete assembly is shown in the accompanying photograph (Figure 4).

The casting unit is shown in the photograph of Figure 5 and in cross section in Figure 6. The tapered crucibles were clamped in place under spring tension between an upper holder and the base plate. The upper and lower supports for the crucible assembly consisted of lengths of 5/8 inch Inconel tubing. The thermocouple leads and a length of 1/8 inch stainless steel tubing carrying argon extended into the crucible through the upper support. The lower support housed a length of 1/4 inch copper tubing, the upper end of which was centered in the tube at a distance of 3/4 inch below the base plate. This copper tube was designed to impinge cold tap water onto the base plate and solidify the alloy unidirectionally from the base.

The bismuth-tin alloys were melted and cast in quartz crucibles mounted upon an aluminum base plate. The high bismuth

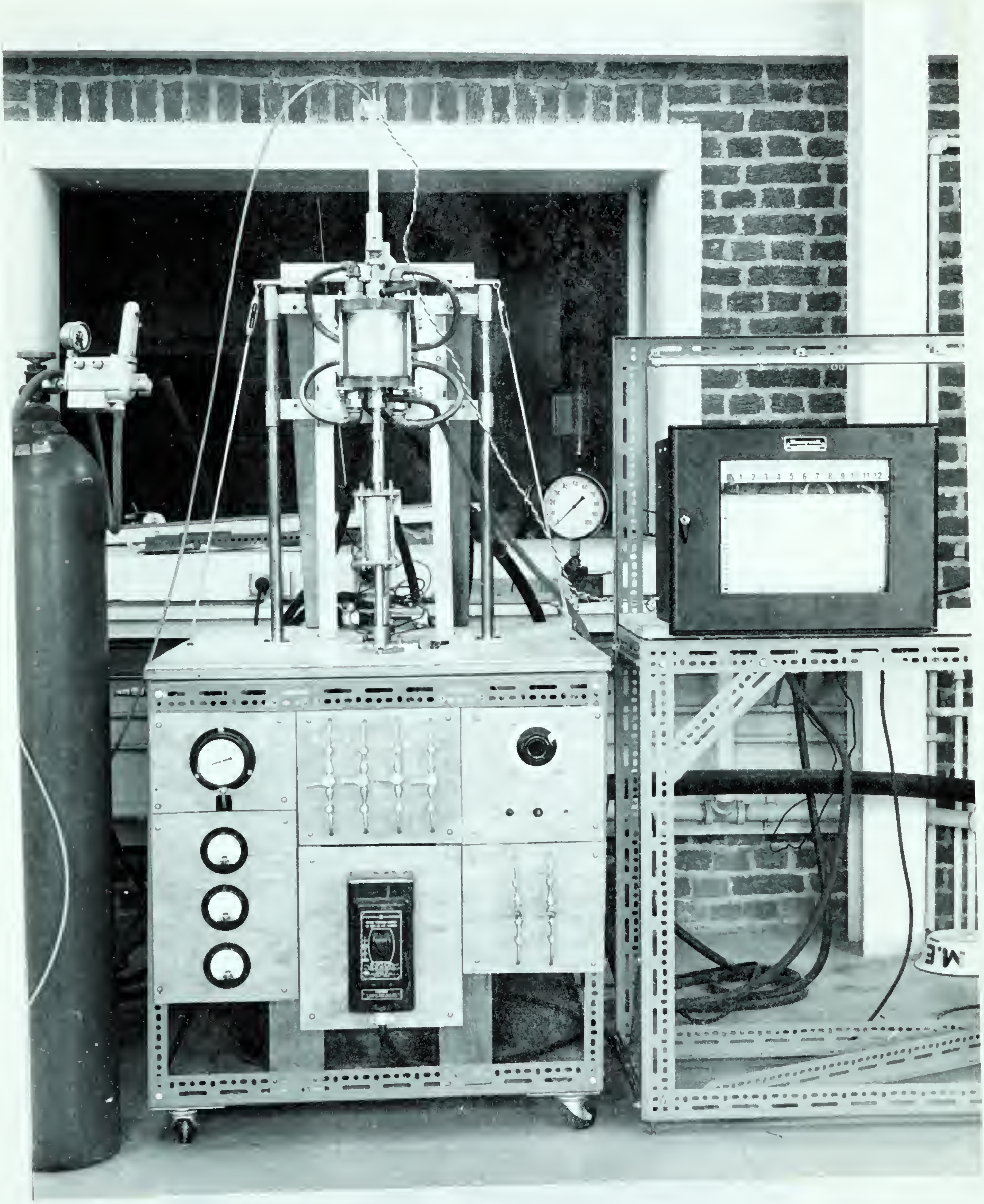

Fig. 4 - Photograph of the Apparatus

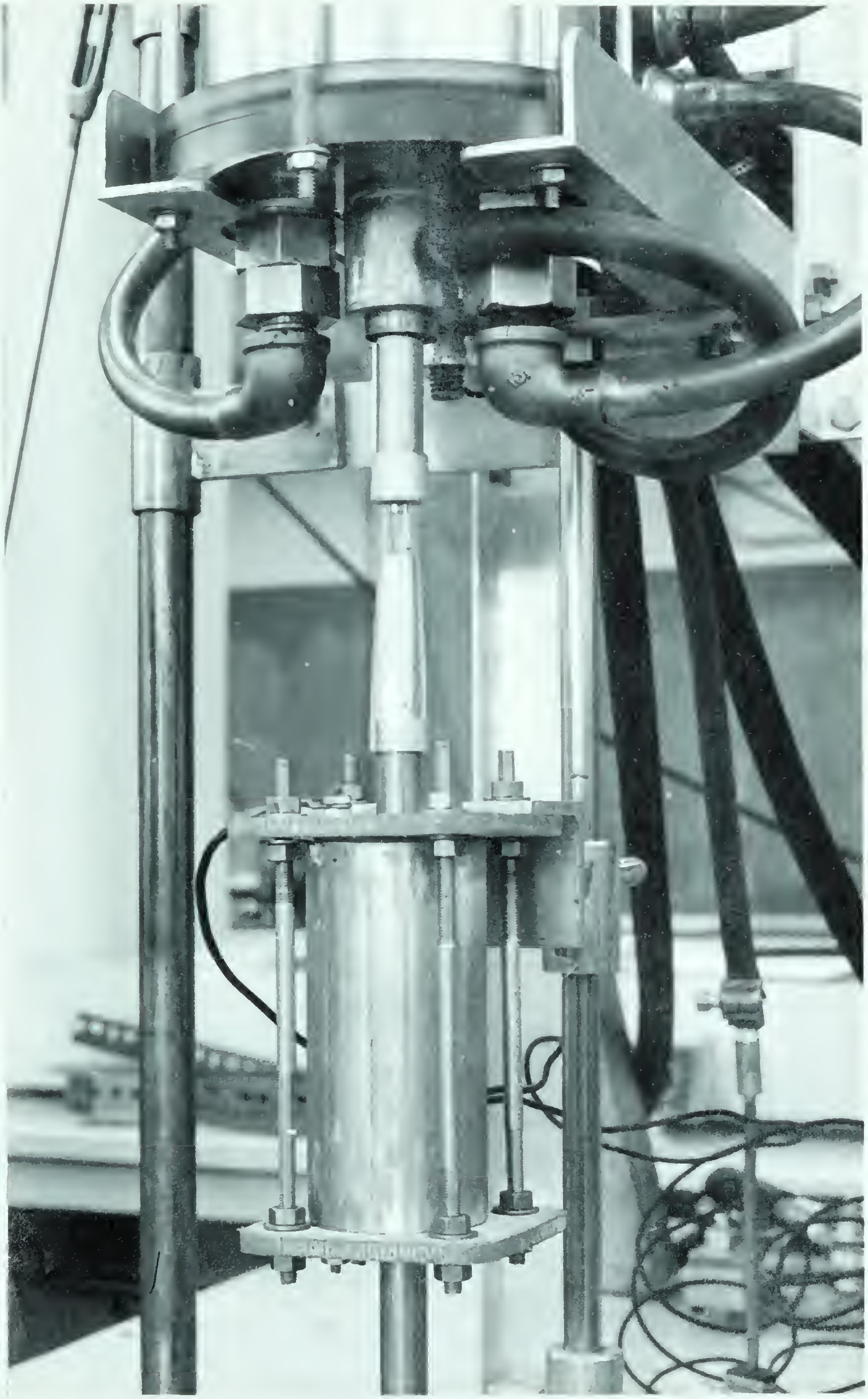

Fig. 5 Photograph of the Casting Unit and Furnace

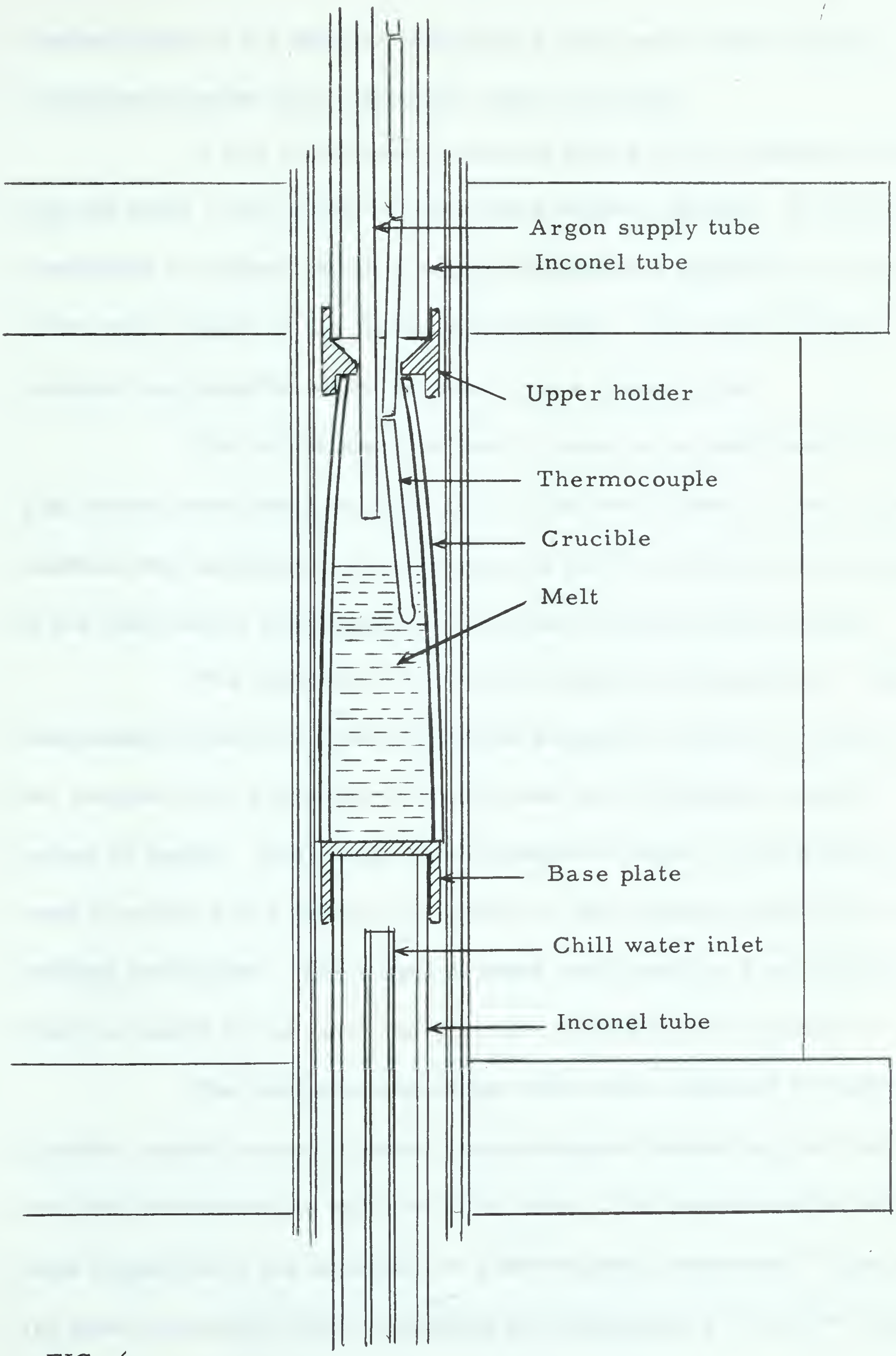

FIG. 6.

Diagram of the Casting Unit.

content alloys of the bismuth-antimony system were cast in quartz crucibles mounted upon a stainless steel base plate.

It was noted upon casting of alloys high in antimony content that the walls of the silica crucible were slightly etched. To avoid the possibility of contamination a change was made to graphite crucibles which were coated on the inside with alundum. The base was also changed to a graphite wafer mounted upon a copper plate.

The alloys were melted by means of a small tube furnace. The furnace was attached to the shaft of the air cylinder by which the solenoid was positioned, an arrangement which facilitated the imposition of the field nearly simultaneously with the removal of the furnace.

The solenoid is discussed in detail in Appendix II. This instrument produced a field of thirteen kilogauss uniform to within a few percent over a cylndrical volume one inch in diameter and two inches in length. The twenty-five kilowatts of direct current power used to produce this field was supplied by two rectifier type direct current welding generators. The output of these machines had a wave form which is shown in the oscilloscope trace reproduced in Figure 7.

The temperatures of the melts were obtained by means of alundum coated chromel-alumel thermocouples located approximately one-half inch below the surface of the melts. The thermocouple leads were connected to the terminals of a Minneapolis-Honeywell "Electronik" six point recorder, which registered the temperature every two seconds

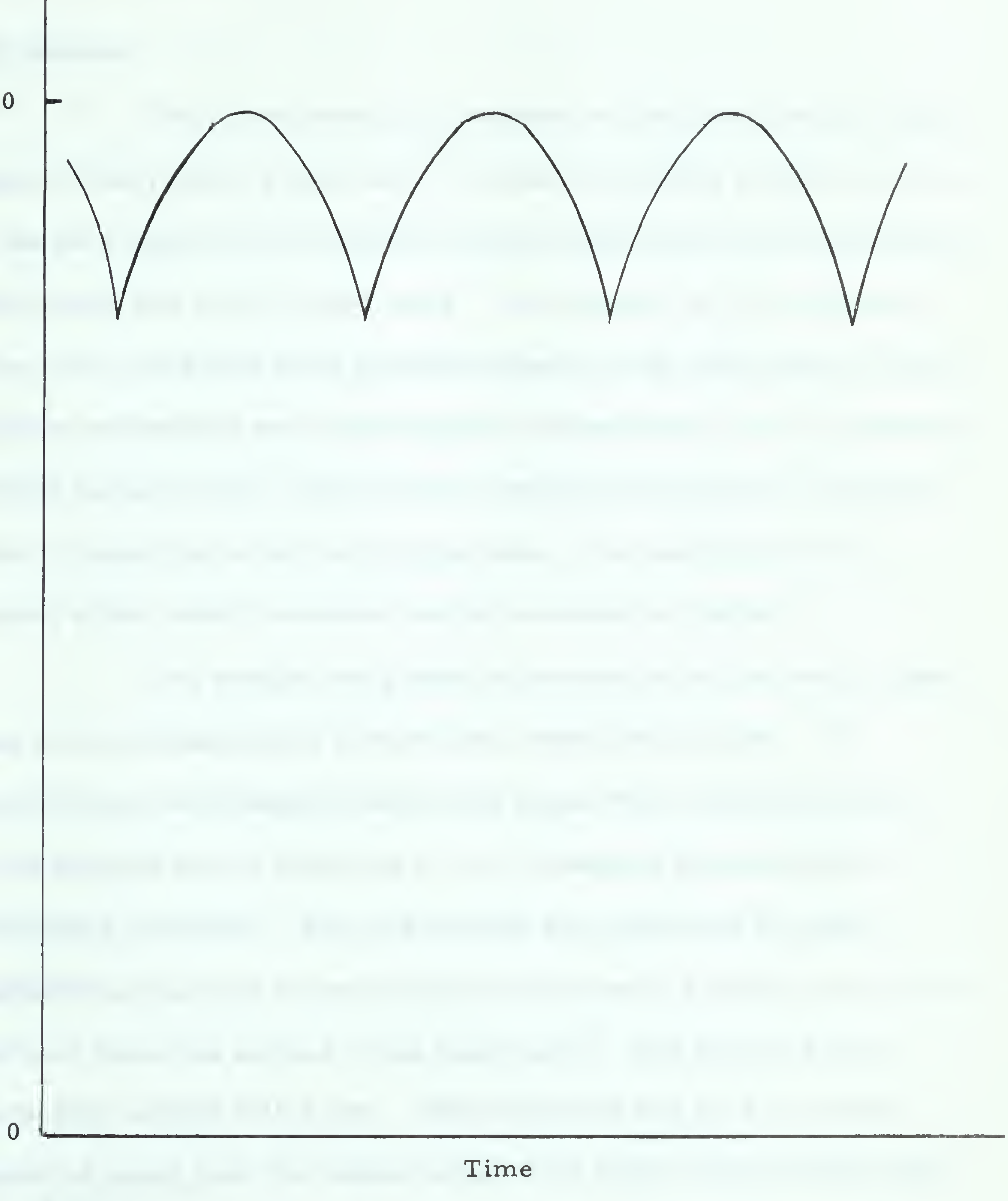

FIG. 7.

Oscilloscope Trace of the Direct Current Output of a Rectifier-Type Welding Generator.
Operating at rated output of 400 A, 40 V. Main ripple 180 cps.
Sweep rate approximately 137 inch/sec.
(Reproduced from mfg. data)

[illegible]

as an imprint on a strip of moving graph paper. The chart speed was one inch per minute.

(2) Method

The alloys were first prepared in the form of small ingots, approximately eighty grams each, by induction melting weighed portions of the pure metals in an alundum crucible under a pure argon atmosphere and casting into a cold copper mold. The bismuth, tin, and antimony from which the alloys were prepared were all of 99.99% purity or better. Further precautions were taken against contamination by first machining a fresh surface on the ingots and then washing with alcohol immediately before remelting in the casting apparatus. The melting and chill casting of the freshly surfaced sample proceeded as follows:

The sample was placed in the crucible of the casting apparatus and the thermocouple lowered into contact with the top. The crucible was then strongly flushed with argon which was kept flowing at the reduced rate of about one c.f.m. throughout the remainder of the casting procedure. The tube furnace was raised and the alloy melted whereupon the thermocouple was lowered to a position about one-half inch below the surface of the liquid metal. The melt was then thoroughly bubbled with argon. This procedure was used to remove dissolved gases from the molten metal which would cause porosity upon cooling and solidifying. The bubbling action also stirred the molten

mass thus enhancing homogeneity. After the bubbling procedure was completed and the temperature was adjusted to fifty degrees of superheat the melt was ready for solidification. In rapid succession the furnace was lowered, the field (which had been previously turned on and adjusted) was imposed and the water jet was impinged on the base to commence the solidification. The field was left on until the ingot was completely solidified and the water jet applied until the ingot was cool to the touch.

The samples were prepared for analysis by sawing each ingot, longitudinally, into sections which were about one-third to two-thirds in proportion. The swarf was collected to serve as the composite ingot sample for analysis. Three cuts, each 0.025 inches in thickness, were milled from the base of each of the larger of the ingot sections to serve as the base samples for chemical analysis.

The methods of analysis are described in detail in Appendix III. All the precautions of good volumetric procedure were applied with the aim of achieving good precision in the analysis between composite and base samples. An estimate of the errors is included in Appendix III.

RESULTS

(1) Metallographic

The macrostructures of the bismuth-antimony ingots are

shown in Figures 8 to 11. The microstructures of the base of the normal and field cast ingots containing 70% bismuth are shown in Figures 12 and 13.

The macrostructures of the bismuth-tin ingots are shown in Figures 14 to 29. The microstructure of the base of the normal and field cast ingots containing 85% bismuth are shown in Figures 30 and 31.

(2) Segregation

The analytical results of the segregation determination for the bismuth-antimony ingots are shown in Figure 34. The theoretical segregation curve is included for comparison. A similar set of curves for the bismuth-tin system (of hyper-eutectic composition) is shown in Figure 35.

The experimental values shown for the segregation in the Bi-Sb ingots represent the extrapolation to the base of the determinations for the three base samples. No corrections for the finite sample size were made for the segregation determinations of the Bi-Sn system since only the chill face samples were analyzed. On the basis of the extrapolation correction made for the Bi-Sb ingots, it is believed that the error incurred by the omission of this correction from the segregation values for the Bi-Sn ingots is less than 0.05%. No exudations were observed on the base of any of the ingots and therefore no corrections were made for this effect.

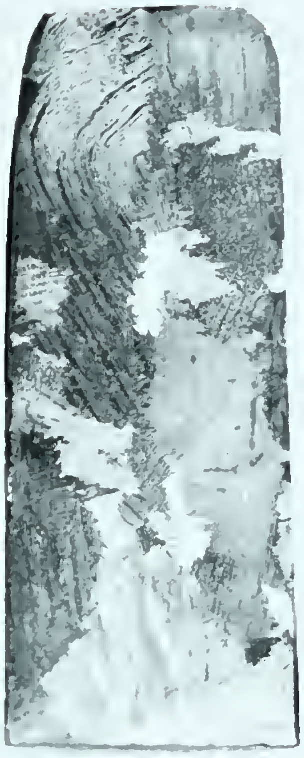

Figure 8 - Normal

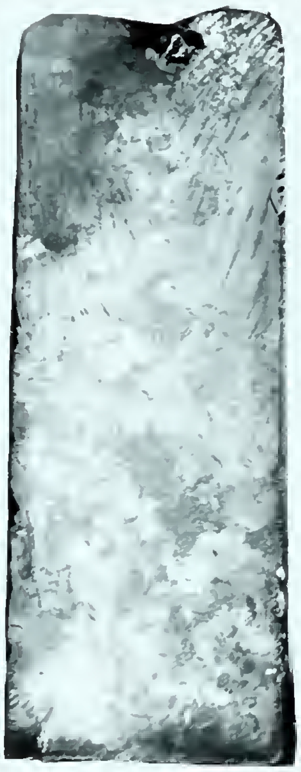

Figure 9 - Field

Macrostructures of the 15% Bi-Sb

Ingots . . . . x 1 1/2

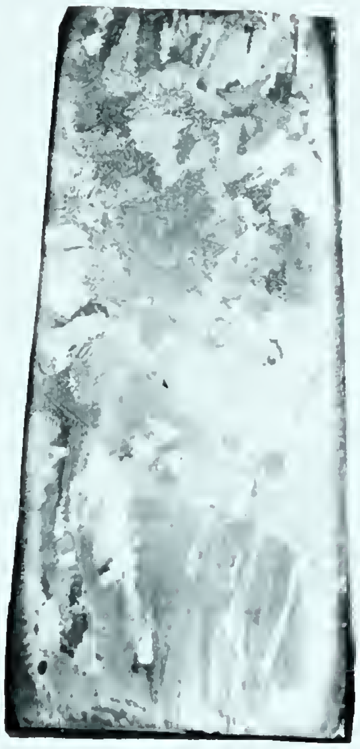

Figure 10 - Normal

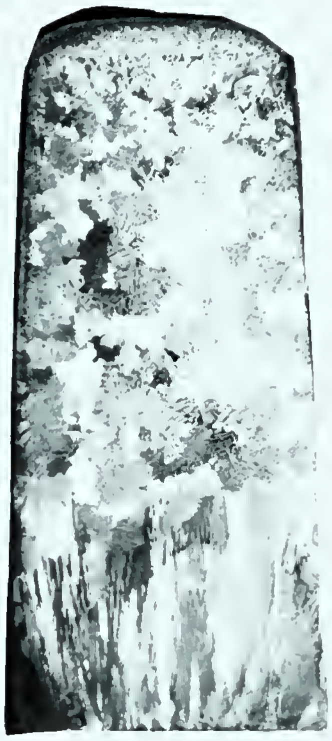

Figure 11 - Field

Macrostructures of the 70% Bi-Sb

Ingots . . . . . x 1 1/2

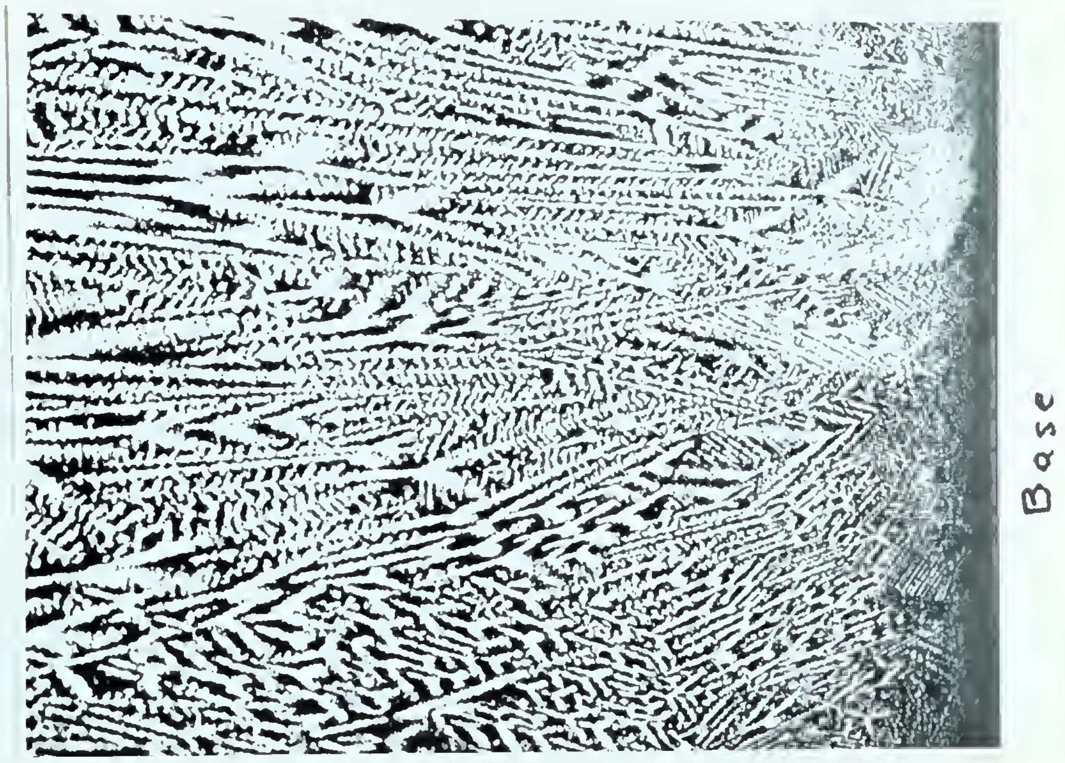

Figure 12 - Microstructure of the Base of

a Normally Cast 70% Bi-Sb Ingot . . . x 250.

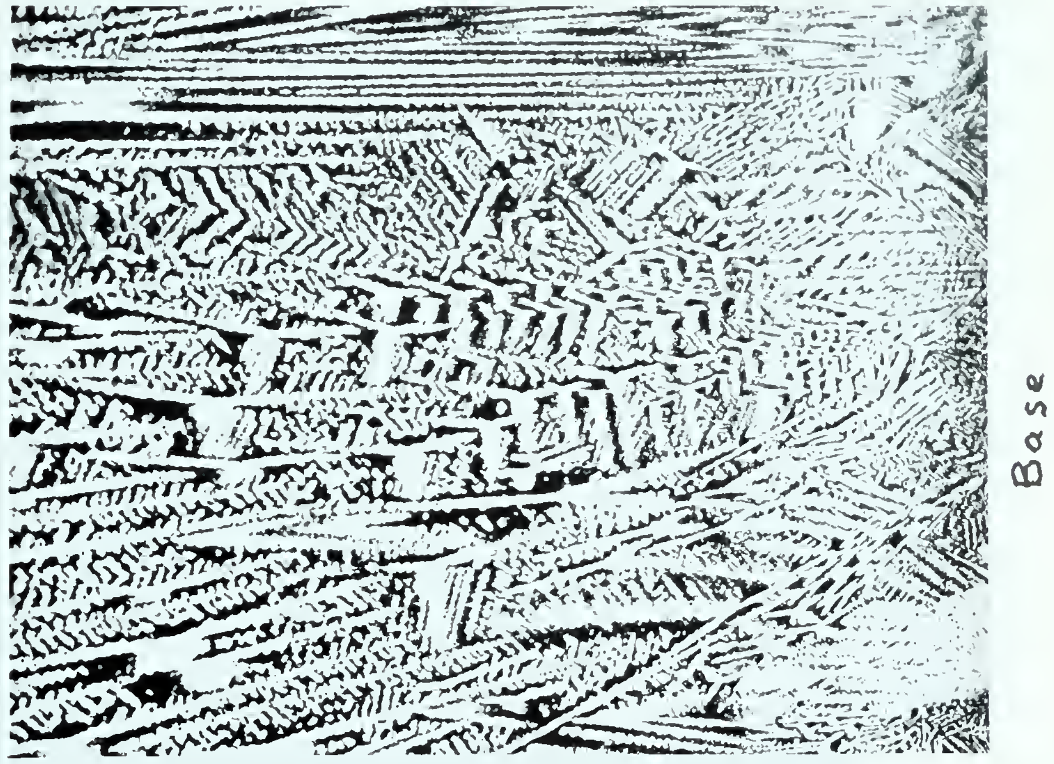

Figure 13 - Microstructure of the Base of

a Field Cast 70% Bi-Sb Ingot . . . x 250.

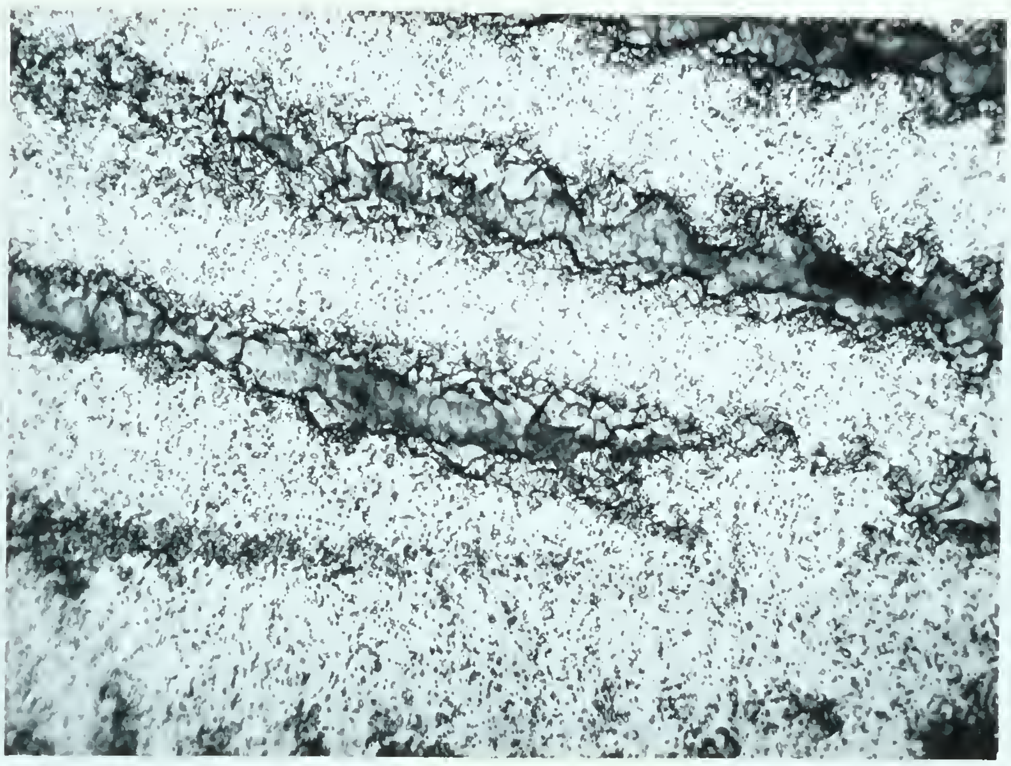

Figure 12a - Microstructure of a Normally Cast 70% Bi-Sb Ingot .... x 600

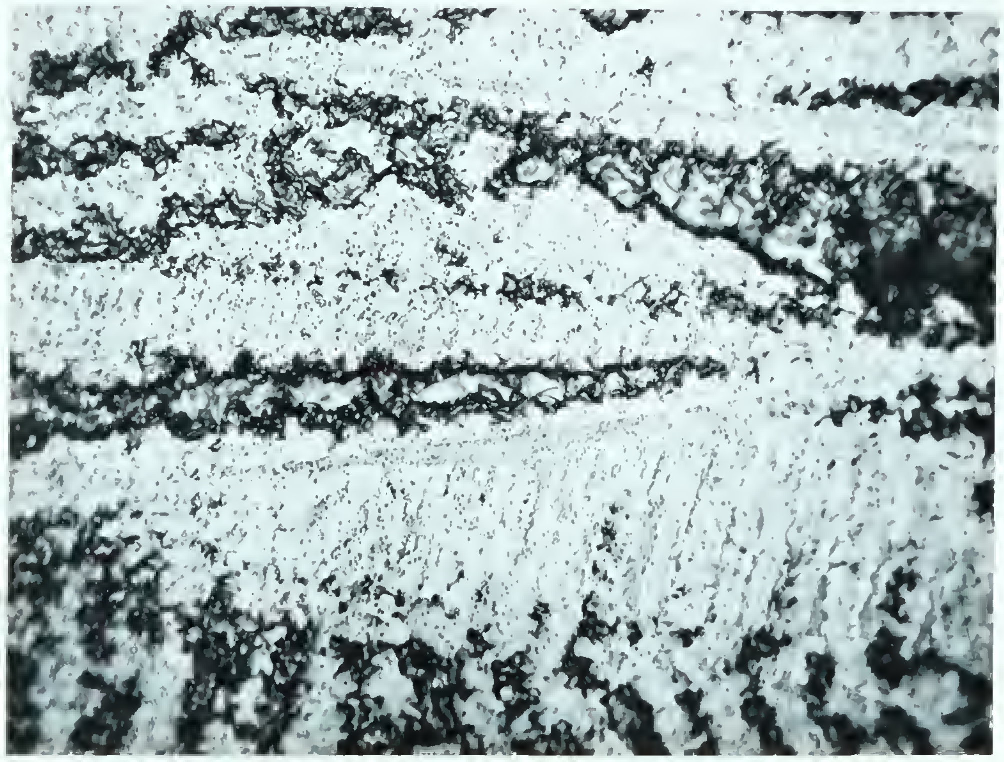

Figure 13a - Microstructure of a Field Cast 70% Bi-Sb Ingot .... x 600

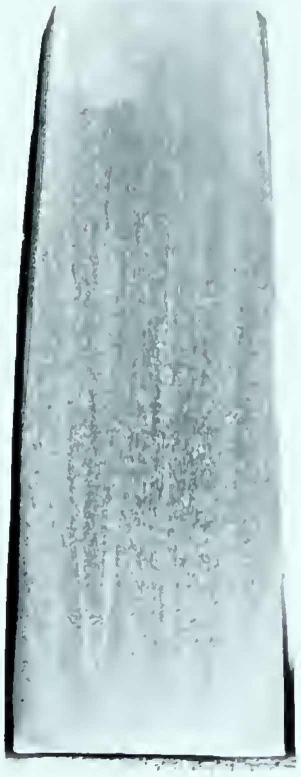

Figure 14 - Normal

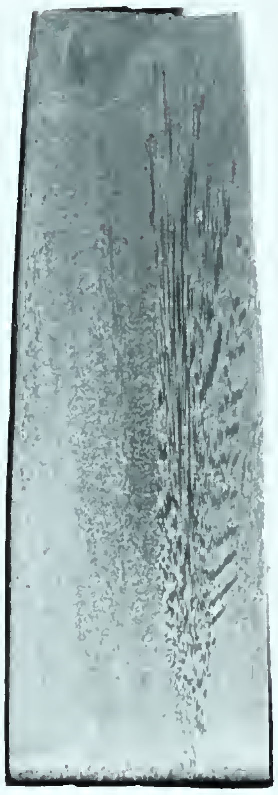

Figure 15 - Field

Macrostructures of the 15% Bi-Sn

Ingots . . . . . x 1 1/2

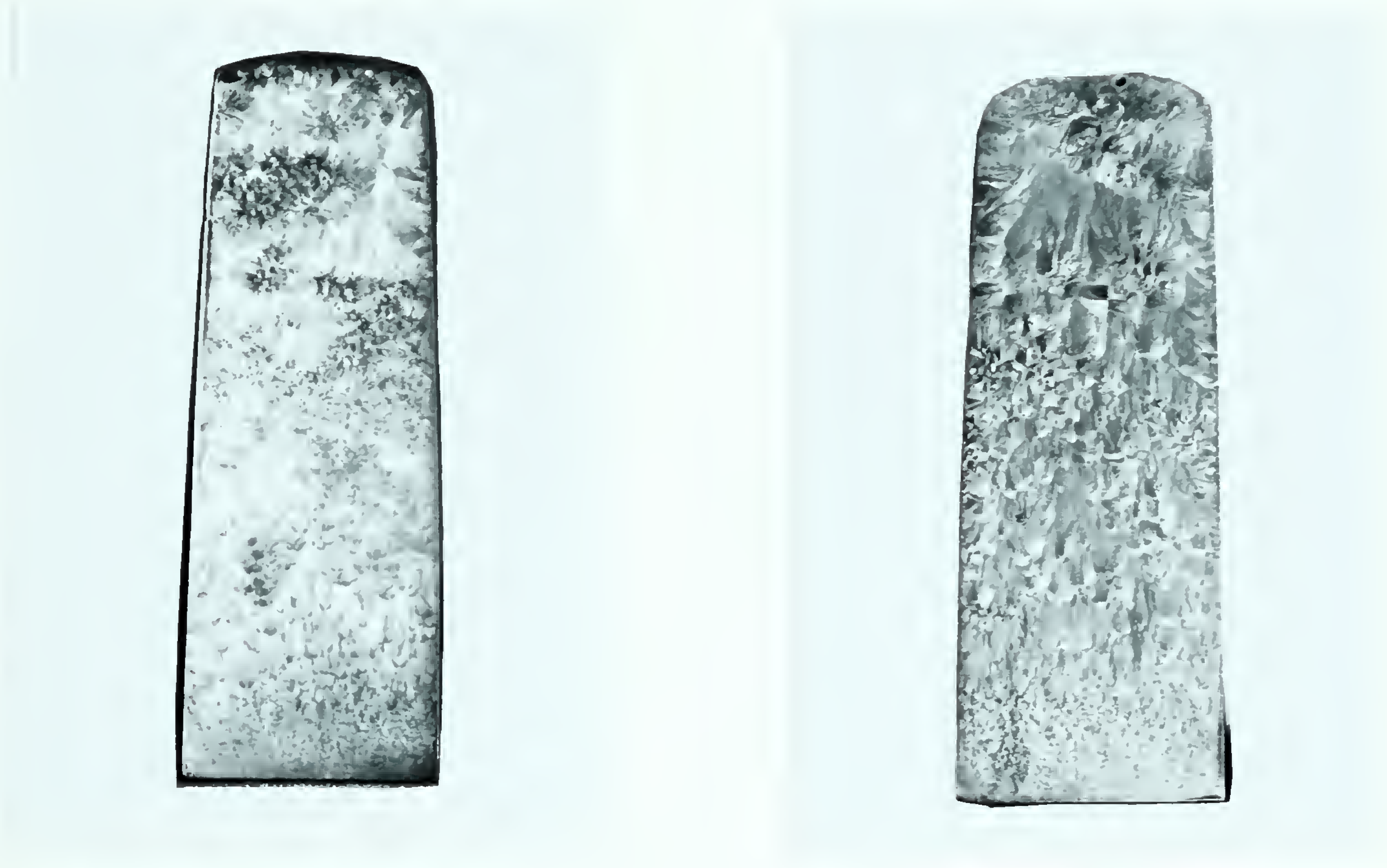

Figure 16 - Normal

Figure 17 - Field

Macrostructures of the 60% Bi-Sn

Ingots . . . . x 1 1/2

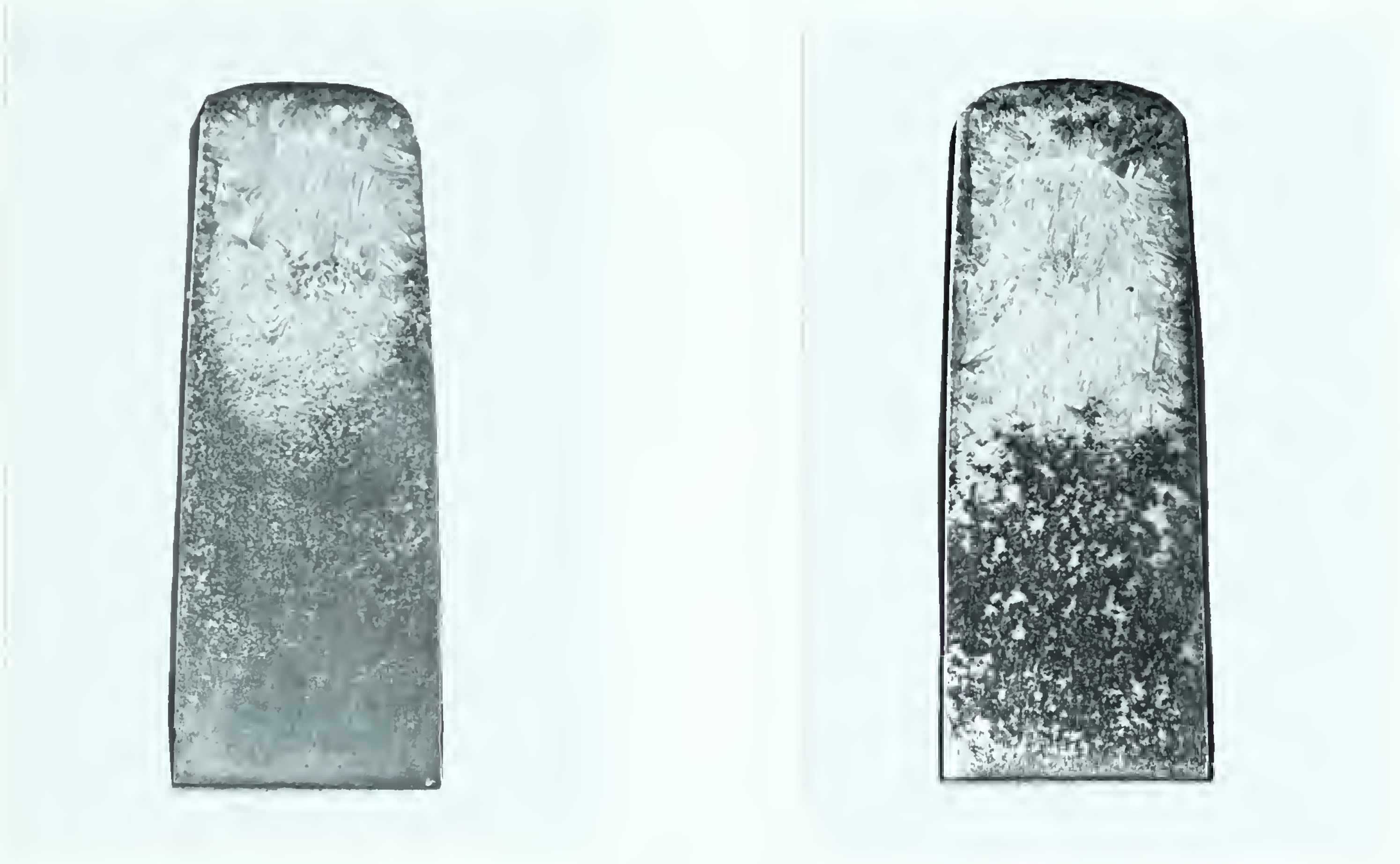

Figure 18 - Normal

Figure 19 - Field

Macrostructures of the 70% Bi-Sn

Ingots . . . . . x 1 1/2

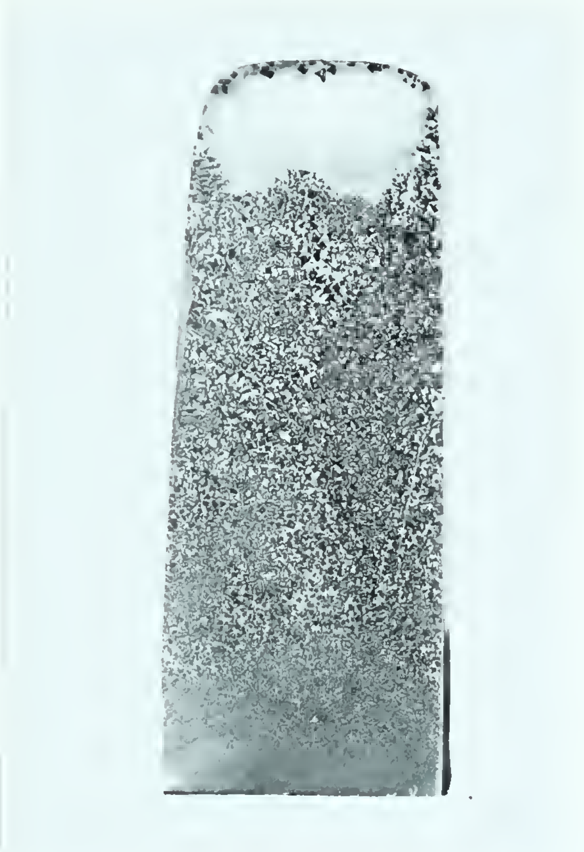

Figure 20 - Normal

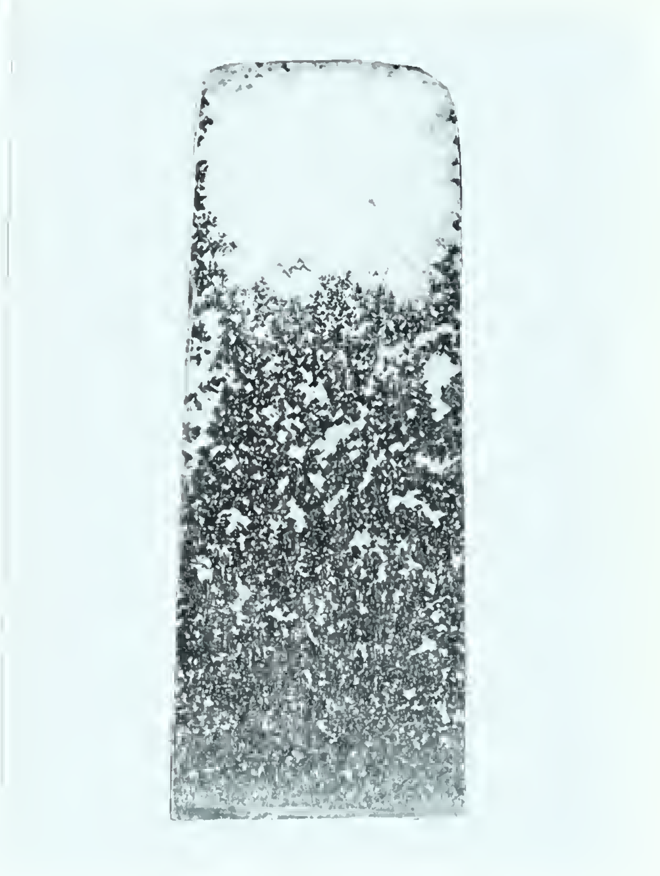

Figure 21 - Field

Macrostructures of the 80% Bi-Sn

Ingots . . . . . x 1 1/2

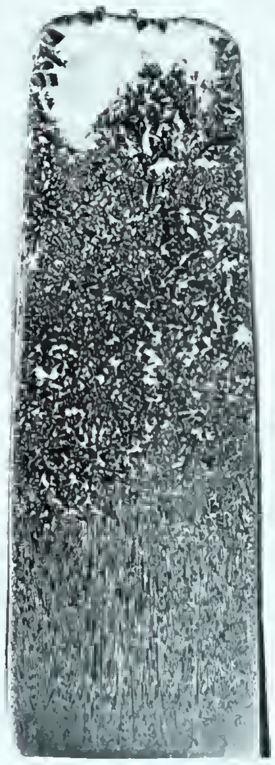

Figure 22 - Normal

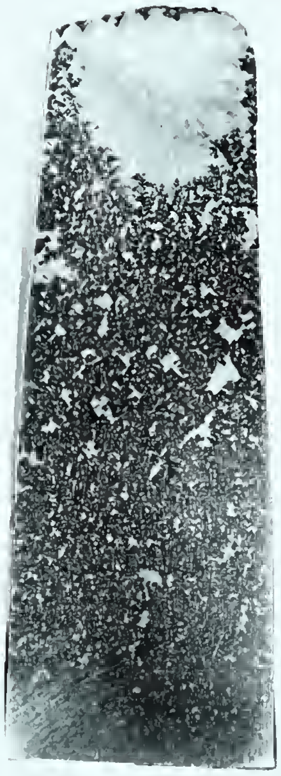

Figure 23 - Field

Macrostructures of the 85% Bi-Sn

Ingots . . . . . x 1 1/2

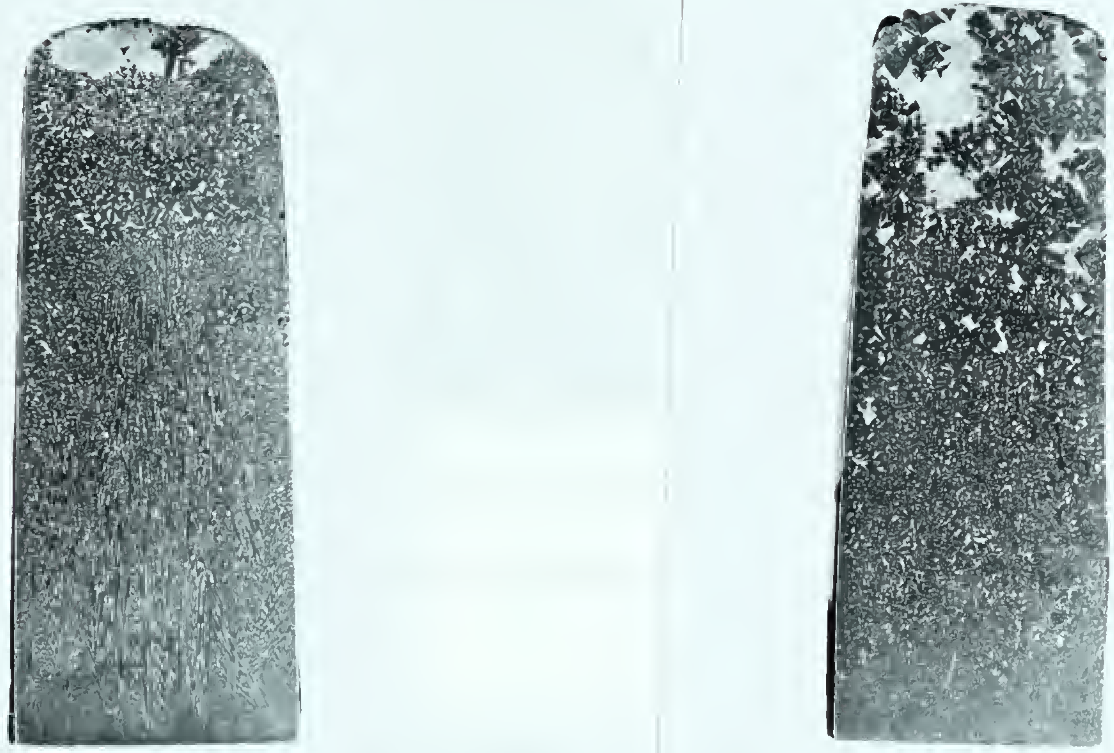

Figure 24 - Normal

Figure 25 - Field

Macrostructures of the 90% Bi-Sn

Ingots . . . . . x 1 1/2

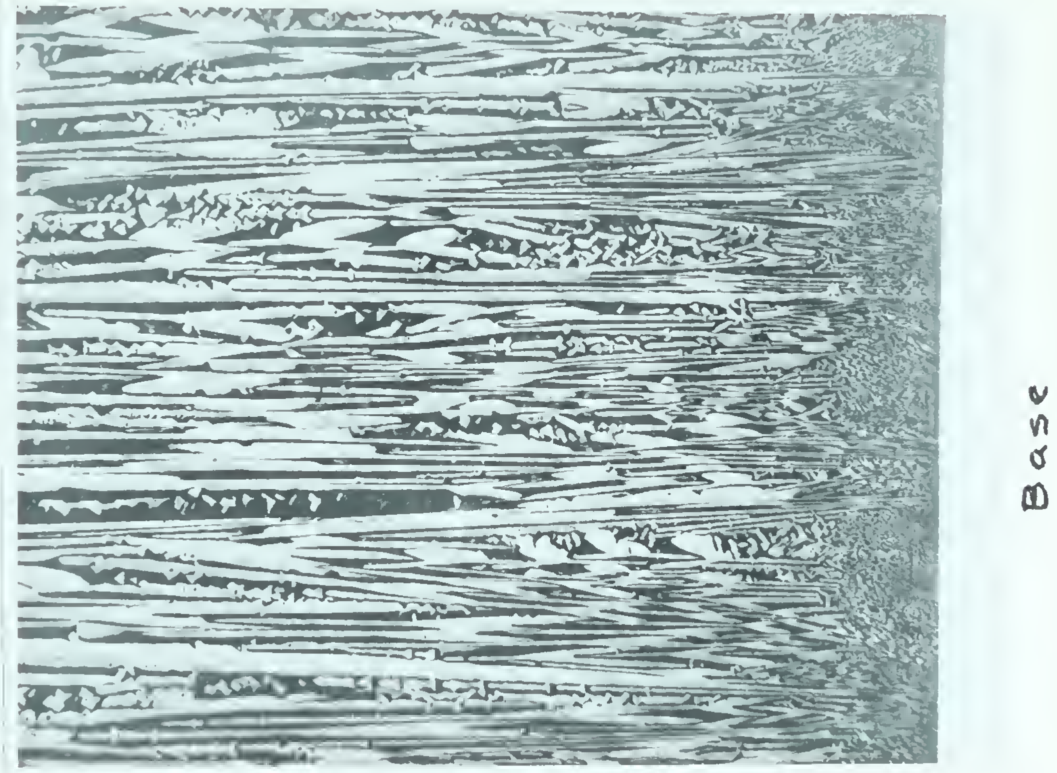

Figure 26 - Macrostructure of the Base of a Normally Cast 85% Bi-Sn Ingot Showing Dendritic Growth . . . . . x 20.

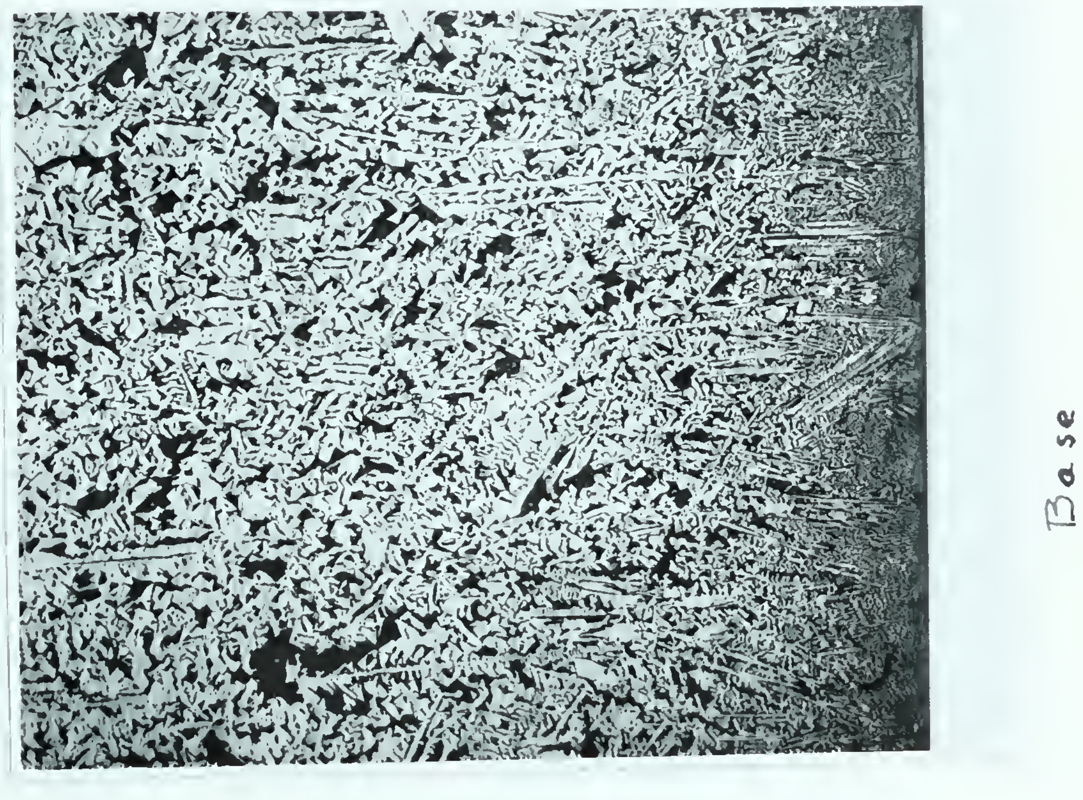

Figure 27 - Macrostructure of the Base of a Field Cast 85% Bi-Sn Ingot Showing Partial Destruction of the Dendrites by the Field . . . x 20.

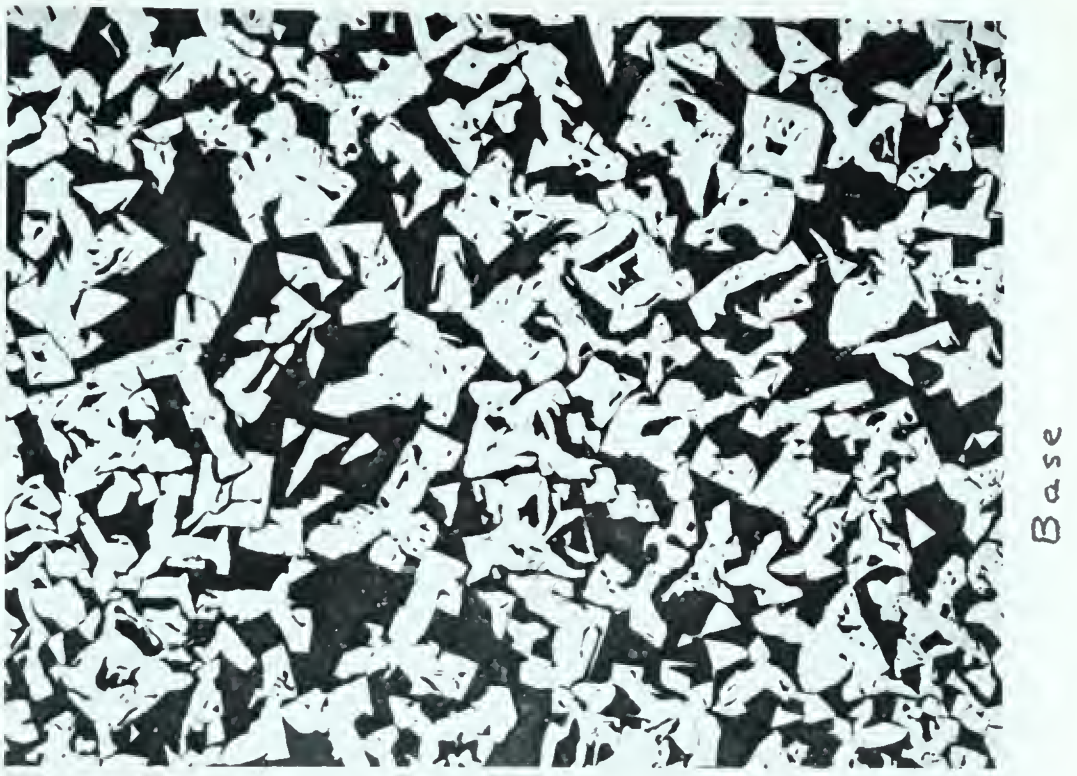

Figure 28 - Macrostructure of the Equiaxial Crystals Occurring at the Center of a Normally Cast 85% Bi-Sb Ingot . . . . . x 20

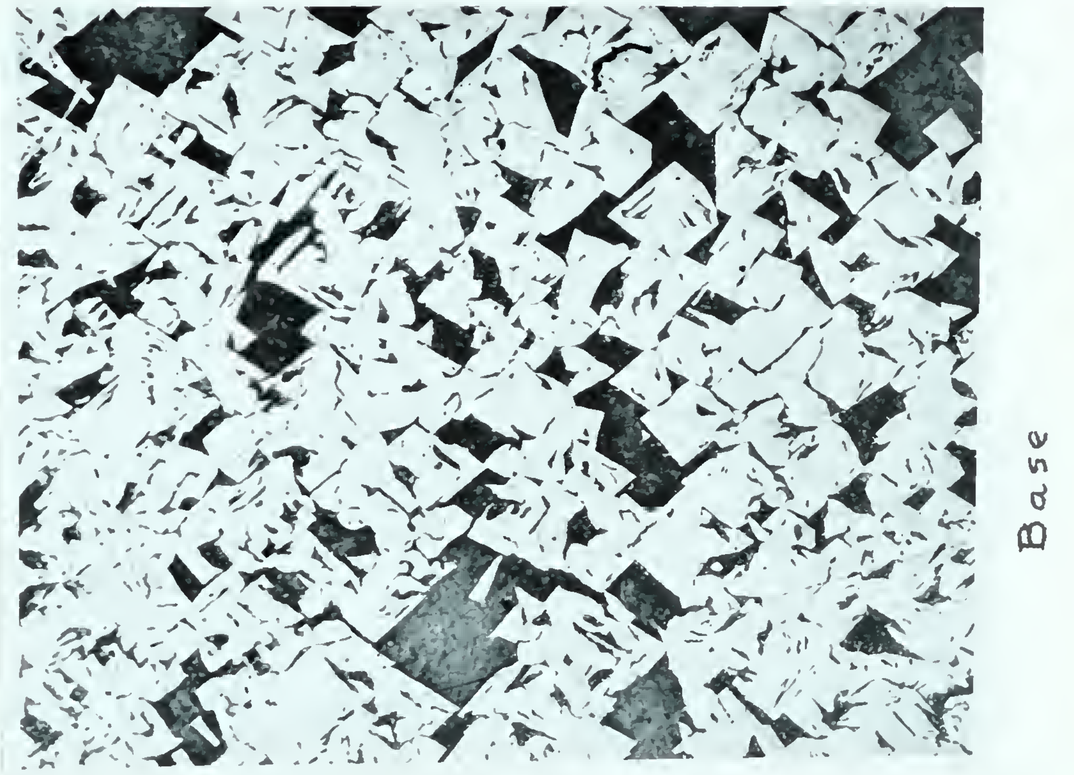

Figure 29 - Macrostructure of the Equiaxial Crystals Occurring at the Center of a Field Cast 85% Bi-Sb Ingot Showing Orientation by the Field . . . . . x 20.

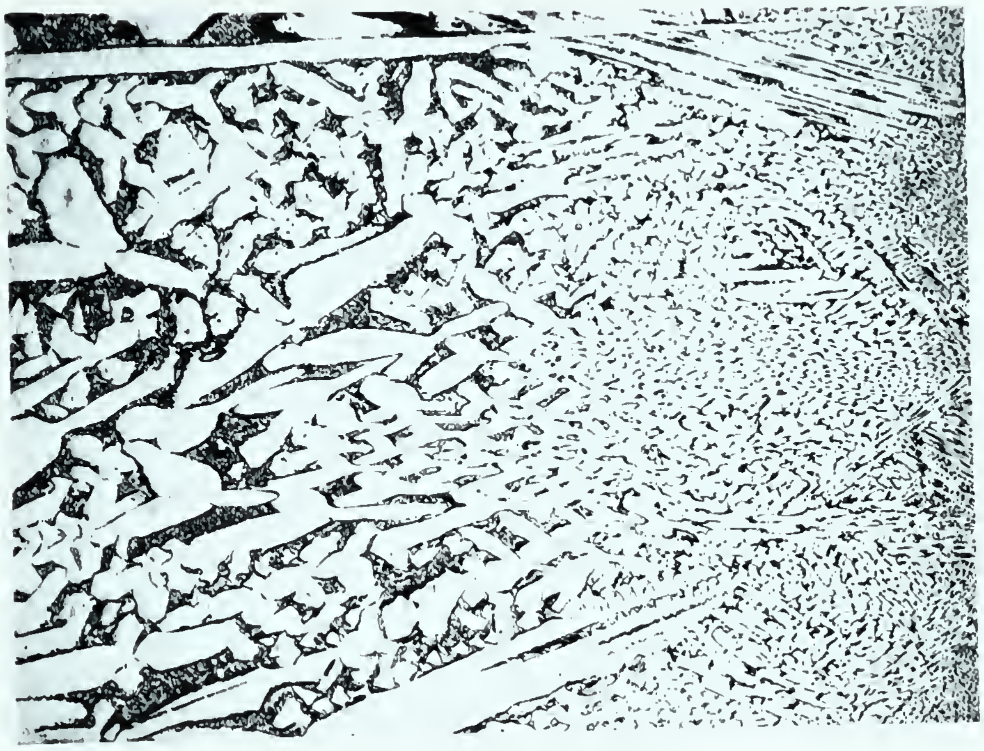

Figure 30 - Microstructure of the Base of a Normally Cast 85% Bi-Sn Ingot . . . . . x 100.

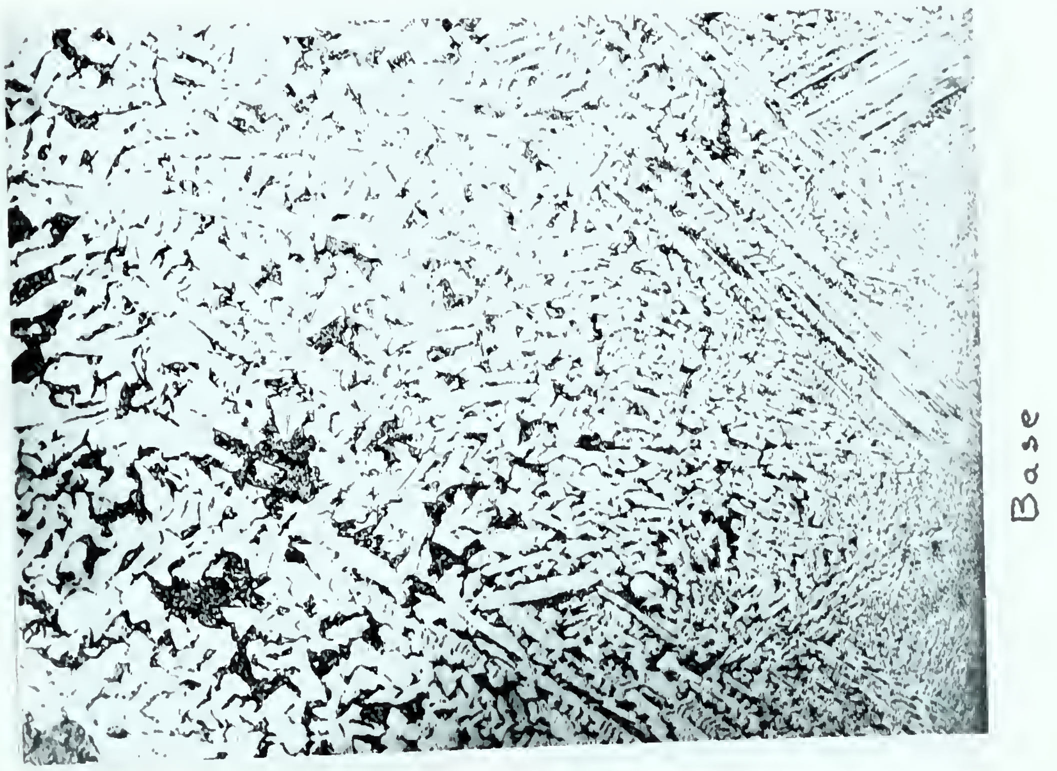

Figure 31 - Microstructure of the Base of a Field Cast 85% Bi-Sn Ingot . . . . . x 100.

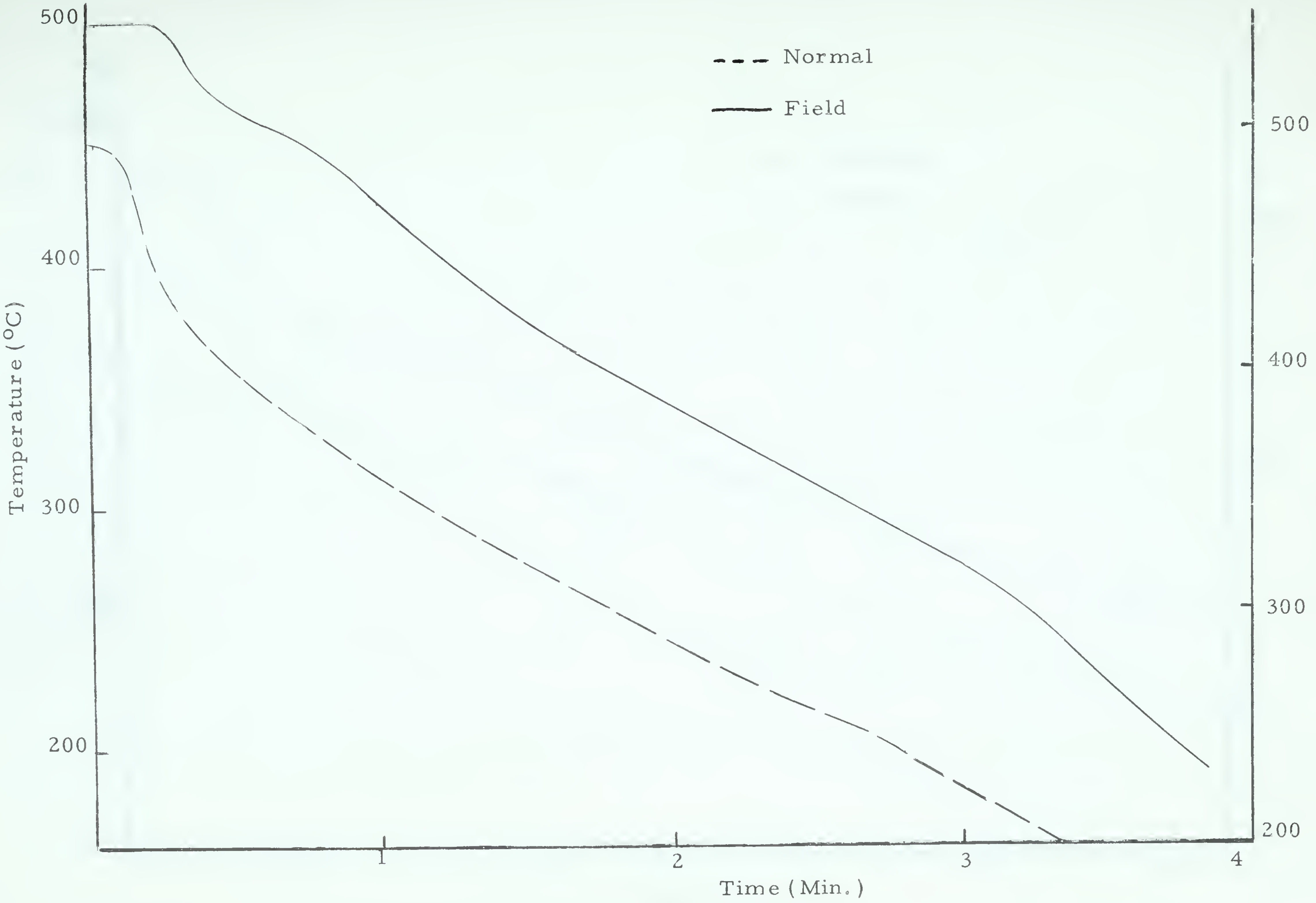

Fig. 32 - Cooling Curves for 70% Bi-Sb Alloys.

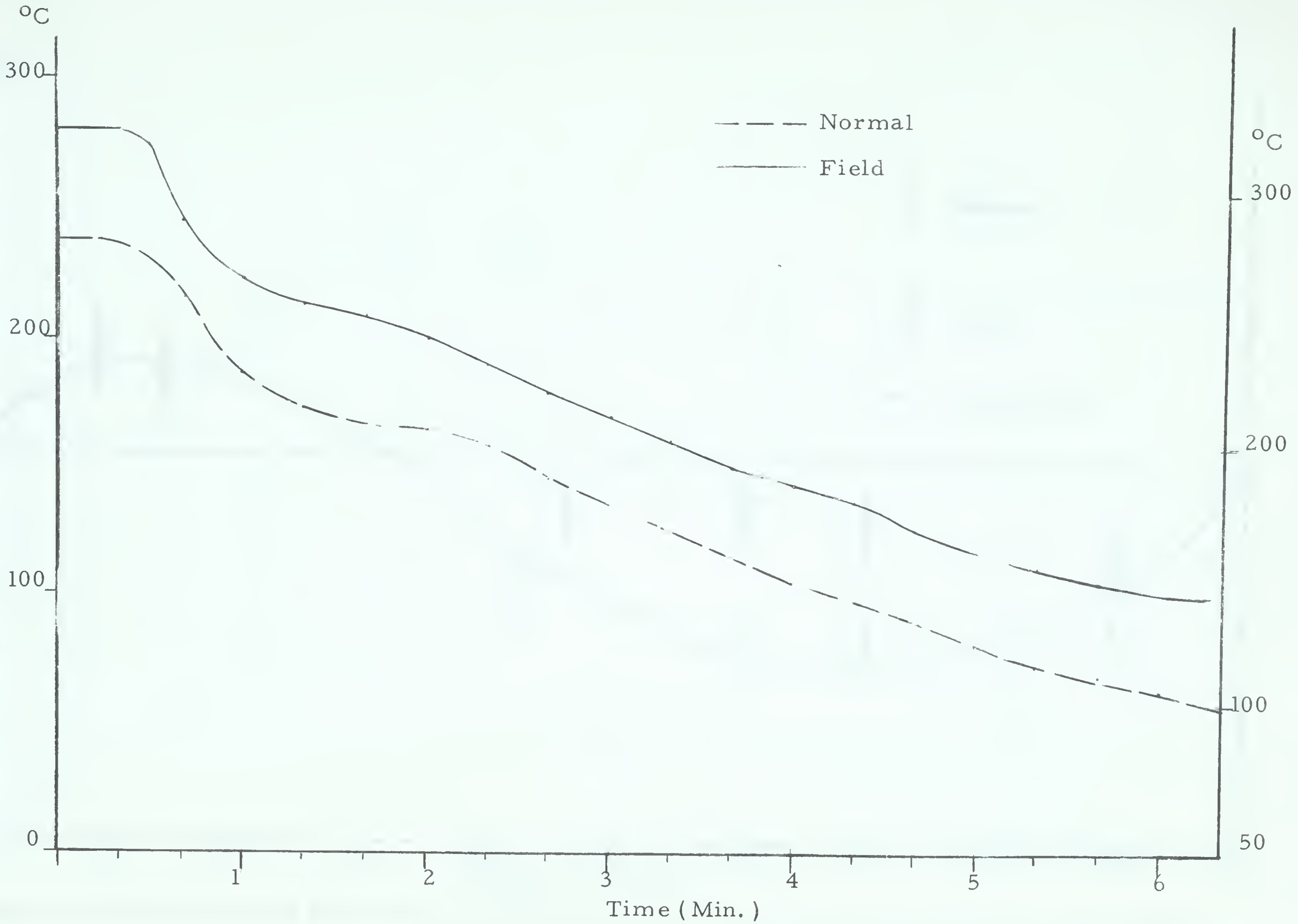

Fig. 33 - Cooling Curves for 85% Bi-Sn Alloys.

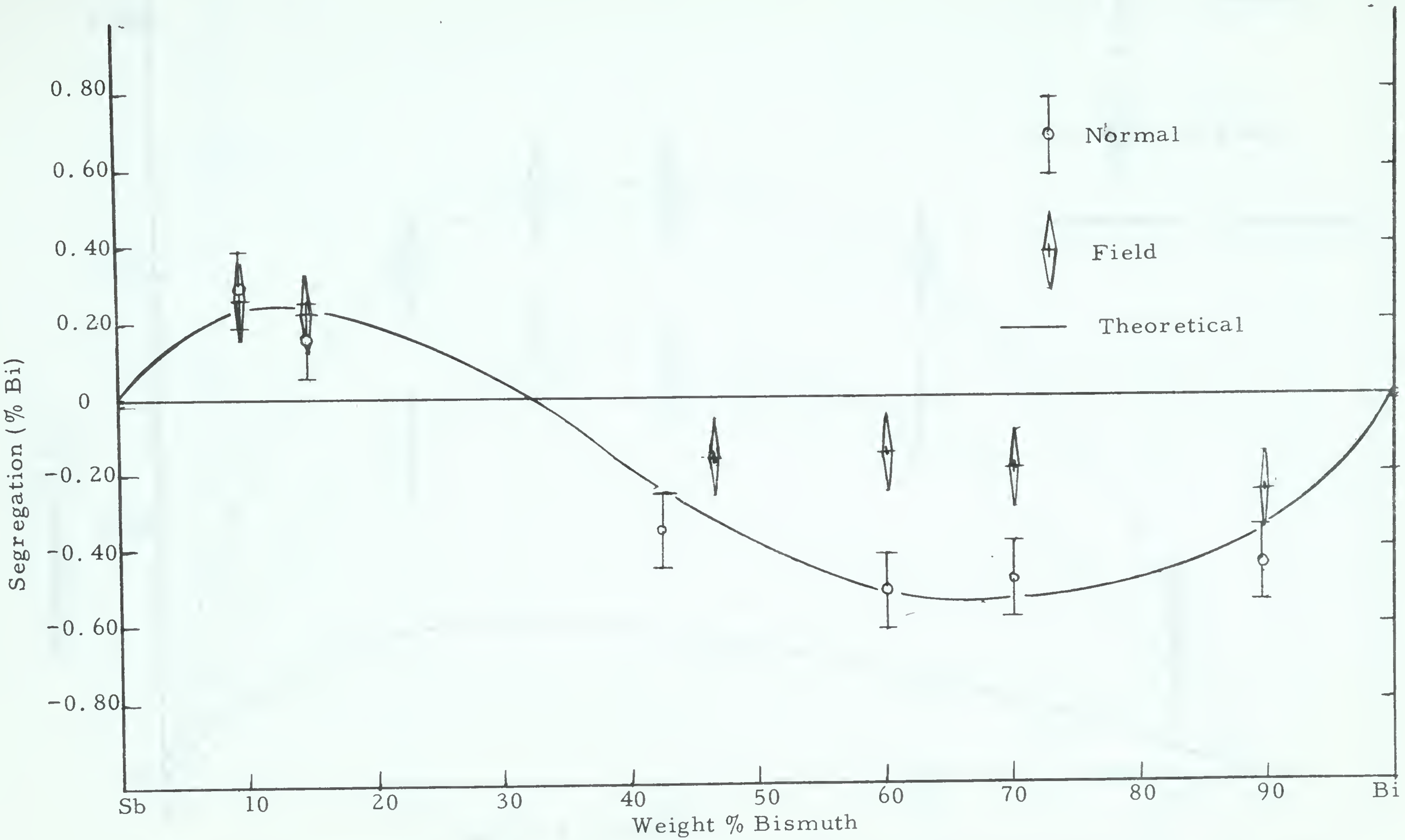

Fig. 34 - Theoretical and Experimental Segregation Curves for the System Bi-Sb. The vertical extension of the points indicates the experimental error.

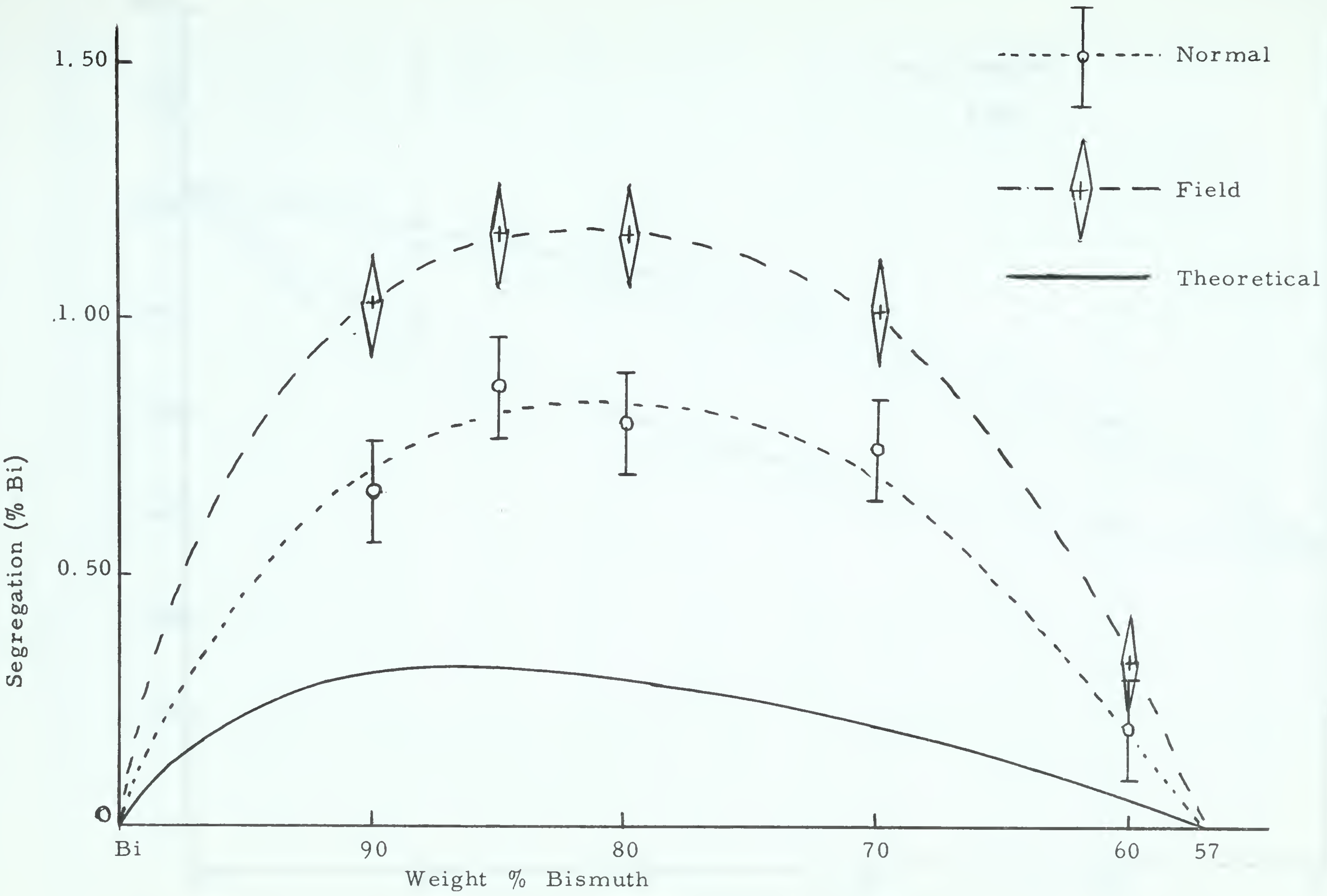

Fig. 35 - Theoretical and Experimental Segregation Curves for the System Bi-Sn. The vertical extension of the points indicates the experimental error.

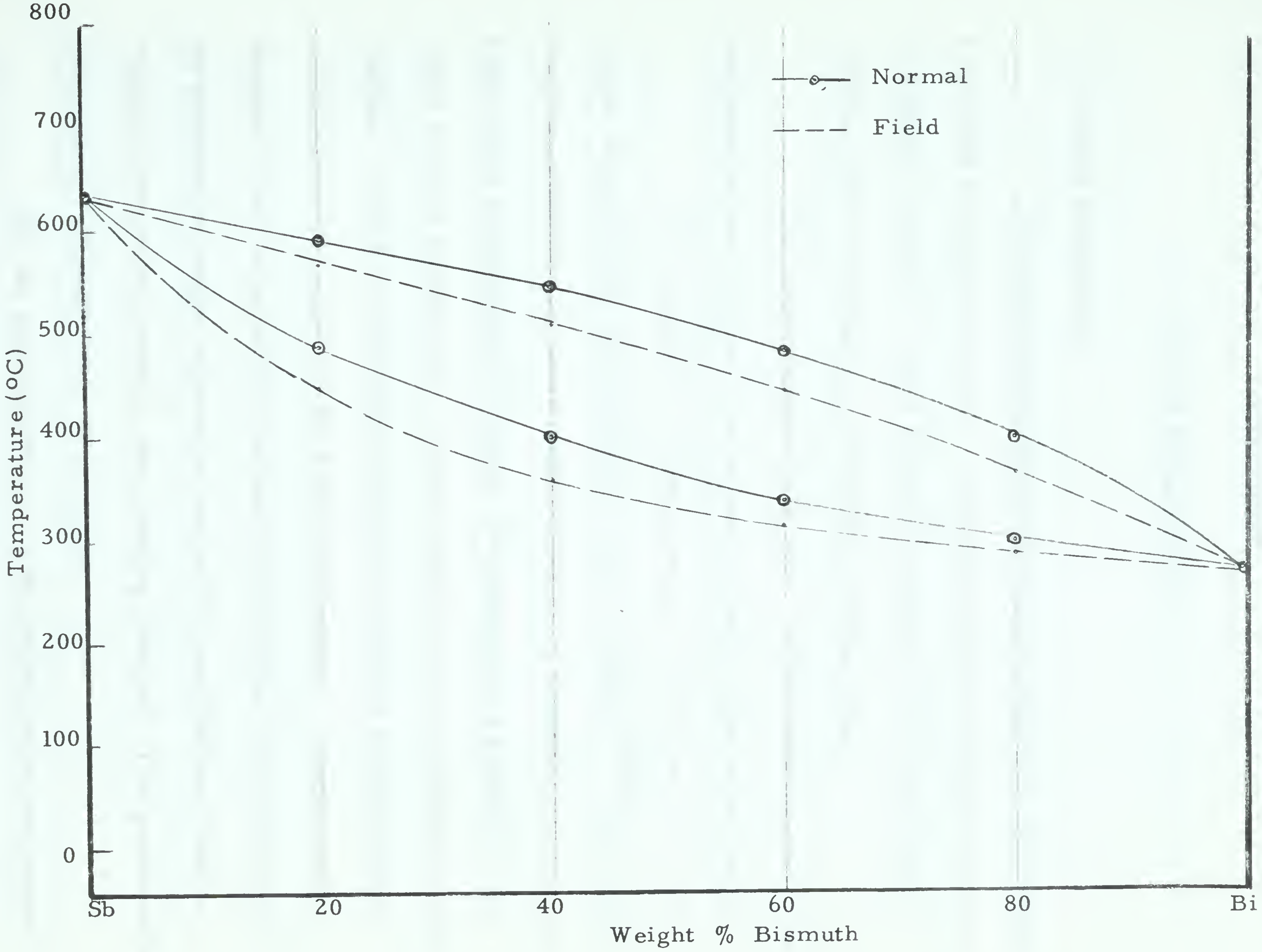

Fig. 36 - Normal and "Field" Equilibrium Diagrams for the System Bi-Sb.

DISCUSSION

A. The System Bi-Sb

(1) Crystal Morphology

The macrostructures of the ingots containing 70% bismuth are shown in Figures 10 and 11. The base microstructures are shown in Figures 12 and 13. These ingots are typical of chill cast alloys in that they show the presence of three well defined zones:

(1) A very narrow chill zone. In this zone the grains are nucleated on the chill face in a narrow thermally supercooled region.

(2) A dendritic columnar zone. On the basis of constitutional supercooling considerations, Tiller and Rutter$^{(26)}$ have shown that the conditions that favor the development of dendritic freezing are appreciable concentration of solute, low temperature gradient in the liquid and high freezing rate. These conditions were satisfied by these castings. There is competition among the dendrites having different orientations with respect to the heat flow direction. Crystals with a dendrite direction parallel to the heat flow direction grow farther into the supercooled region adjacent to the solid-liquid interface than less favorably orientated crystals, thus choking them off. This produced the well oriented columnar zone in the ingots.

(3) An equiaxial zone. As the solidification progresses, the temperature gradient decreases. This increases the supercooling

until the liquid is cooled sufficiently that nucleation occurs ahead of the dendrite tips. This creates a zone of equiaxial crystals.

The field cast 70% Bi-Sb ingot has a somewhat finer grain structure in the equiaxial zone than the normally cast ingot of the same composition. The finer grain is probably due to increased nucleation. This would occur if the liquid ahead of the advancing interface was supercooled to a greater degree in the field cast ingot than in the normally cast ingot. The magnetic field reduced the thermal conductivity of the alloy and this resulted in a somewhat lower cooling rate for the field cast ingot (see Figure 32 - the field cast ingot cooled at an average rate of 80°C/min. compared to 88°C/min. for the normally cast ingot). If the reduction in the cooling rate was just sufficient to lower the thermal gradient in the liquid this would increase the supercooling (see Figure 1). The alternation of the field may also have produced some mixing of the liquid. In general this would increase the grain size which is contrary to what is observed for this case.

The macrostructures of the normally cast and field cast ingots containing 15% bismuth are shown in Figures 8 and 9. The normally cast ingot shows some evidence of a columnar zone but consists largely of equiaxial crystals produced by nucleation in supercooled liquid ahead of the advancing interface. The field cast ingot again shows a finer equiaxial grain structure than the normally cast ingot. The explanation given above for the finer grain structure of the field cast 70% Bi-Sb ingot is assumed to hold also for this case.

(2) Segregation

Good agreement was obtained between the theoretical and experimental segregation values for the normally cast ingots (see Figure 32). The positive segregation which occurred at the base of the antimony-rich ingots is a result of the contraction upon solidification of the primary dendrites followed by drawback of the bismuth-rich residual liquid. As the bismuth content of the ingots increases there is a change from contraction to expansion upon solidification of the primary dendrites. This effect, coupled with the expansion upon solidification of the bismuth-rich residual liquid, resulted in the negative segregation observed at the base of the bismuth-rich ingots.

The segregation which occurred at the base of the ingots cast in the magnetic field was significantly less, for ingots of appreciable bismuth content, than that which occurred under normal casting conditions. This change in segregation was related to a "field equilibrium diagram" by means of the equations of the inverse segregation theory (see Appendix I). The effect of a variation in the parameters "a" and "A" on the segregation is shown by the following expressions for the mass terms:

The liquid remaining at the final temperature of solidification

$$m_{sE} \sim \prod_{i} \left(\frac{c_{s_{i+1}}}{c_{s_i}} \right)^{-\frac{a_i}{A_i}}$$

The mass of bismuth in the cored primary crystals -

$$m_{kE}\, C_{kE} \sim \sum_{i} \left(m_{s_i} \; c_{s_i}\right) \left[\left(\frac{c_{s_{i+1}}}{c_{s_i}} \right)^{\frac{A_i - a_i}{A_i}} - 1 \right]$$

In general for this system

(1) Increasing the separation of the liquidus and solidus lines increases "A" and results in an increase in the amount of liquid remaining at the final solidification temperature.

(2) Varying the shape of the lines but keeping their separation constant varies the amount of expansion or contraction of the primary crystals.

A series of trial calculations based on these general effects established the field equilibrium diagram (Figure 36) which corresponds to the segregation observed in the field cast ingots. Some verification of this explanation of the change in the segregation induced by the field, by means of an altered phase diagram, is given by the differences observed in the coring between normally cast and field cast ingots (see Figures 12a and 13a).

The possible influence on the segregation in the field cast ingots of the fluctuations present in the magnetic field should be considered. In Figure 7 it is shown that the current supply to the solenoid alternated about the mean value by approximately ± 10% at a

rate of 180 cps.

The frequency of the alternation was too low to induce heating of the samples but it may have had some mixing effect on the liquid metal. In Appendix I it is stated that complete liquid homogeneity is one of the basic assumptions of the theory of inverse segregation. Any mixing of the liquid which occurred as a result of variations in the magnetic field would further validate this assumption. It is concluded that the fluctuations present in the field would not affect the segregation occurring at the base of the chill cast ingots.

B. The System Bi-Sn

(1) Crystal Morphology

The macrostructures of the bismuth-tin ingots are shown in Figures 14 to 25. For those ingots which are higher in bismuth content than the eutectic composition they illustrate a striking difference in crystal morphology between the ingots cast in the field and those cast under the normal conditions of unidirectional solidification. The various aspects of the ingot structures will now be considered.

(a) The occurrence of well defined regions within the ingots: The areas of the ingots which appear light in color were identified under higher magnification as eutectic. The darker areas are the primary bismuth phase. The distinct separation of these phases in the ingot structure indicates a very high degree of segregation throughout

the length of the ingot. The ingots solidified in the field exhibit a greater separation into primary and eutectic regions than those solidified normally.

The amount of the eutectic phase appearing in the macrostructures is proportional to the composition, as one would expect. The ingots containing 60% of bismuth, which are very close to the eutectic composition of 58% bismuth, show a complete eutectic structure while those containing 90% bismuth show the occurrence of only a very small eutectic area at the top of the ingot.

(b) The zones of the normally solidified ingots: The ingots which are high in bismuth exhibit the three zones commonly occurring in chill castings; a very narrow zone of chill crystals next to the base, a dendritic zone and a zone of equiaxial crystals toward the top of the ingot. The disappearance of the dendritic zone with increased alloy content (Sn) is in accordance with the observations of Cibula(19). As the alloy content increases, so does the degree of constitutional supercooling. Eventually this gives rise to the nucleation of crystallites ahead of the interface, resulting in an equiaxial structure.

(c) The zones of the ingots solidified in the field: The field cast ingots do not exhibit a dendritic zone. They do show a very narrow zone of chill crystals at the base followed by a zone of equiaxial crystals in which the grain size is somewhat larger than that of the equiaxial crystals occurring in the normally cast ingots. The difference in the morphology of the normally cast and field cast ingots may

be due to the following:

(i) A difference in the thermal conductivity of the alloys in the presence of the field

(ii) A conflict between preferred orientation of the crystals in the field and the preferred dendritic growth direction

(iii) Liquid mixing produced by alternation of the field

The cooling rate for the field cast ingots was slightly less than that of the normally cast ingots (see Figure 33 - the field cast 85% Bi-Sn ingot cooled at an average rate of 26°C/min. compared to 29°C/min. for the normally cast ingot). A literature search did not reveal any data for the reduction in the thermal conductivity of bismuth-tin alloys in a magnetic field. Kaye(36) has determined that the thermal conductivity of a bismuth single crystal, $k_{\parallel}$(see Figure 37), is reduced by a factor of 0.975 in a magnetic field of ten kilogauss imposed parallel to the trigonal axis at room temperature. Since the primary crystals formed at the base are very nearly pure bismuth, this factor may be significant. In the equiaxial zone the preferred orientation of the primary bismuth crystals would tend to reduce the longitudinal heat flow (see Figure 37).

A reduction in the thermal conductivity of the solidified mass at the base of the ingots would decrease the supercooling in the liquid ahead of the advancing interface and result in larger equiaxed crystals as observed (compare Figures 18 & 19). However, the observed difference in cooling rates is not considered to be sufficiently large to completely account for the difference in grain size.

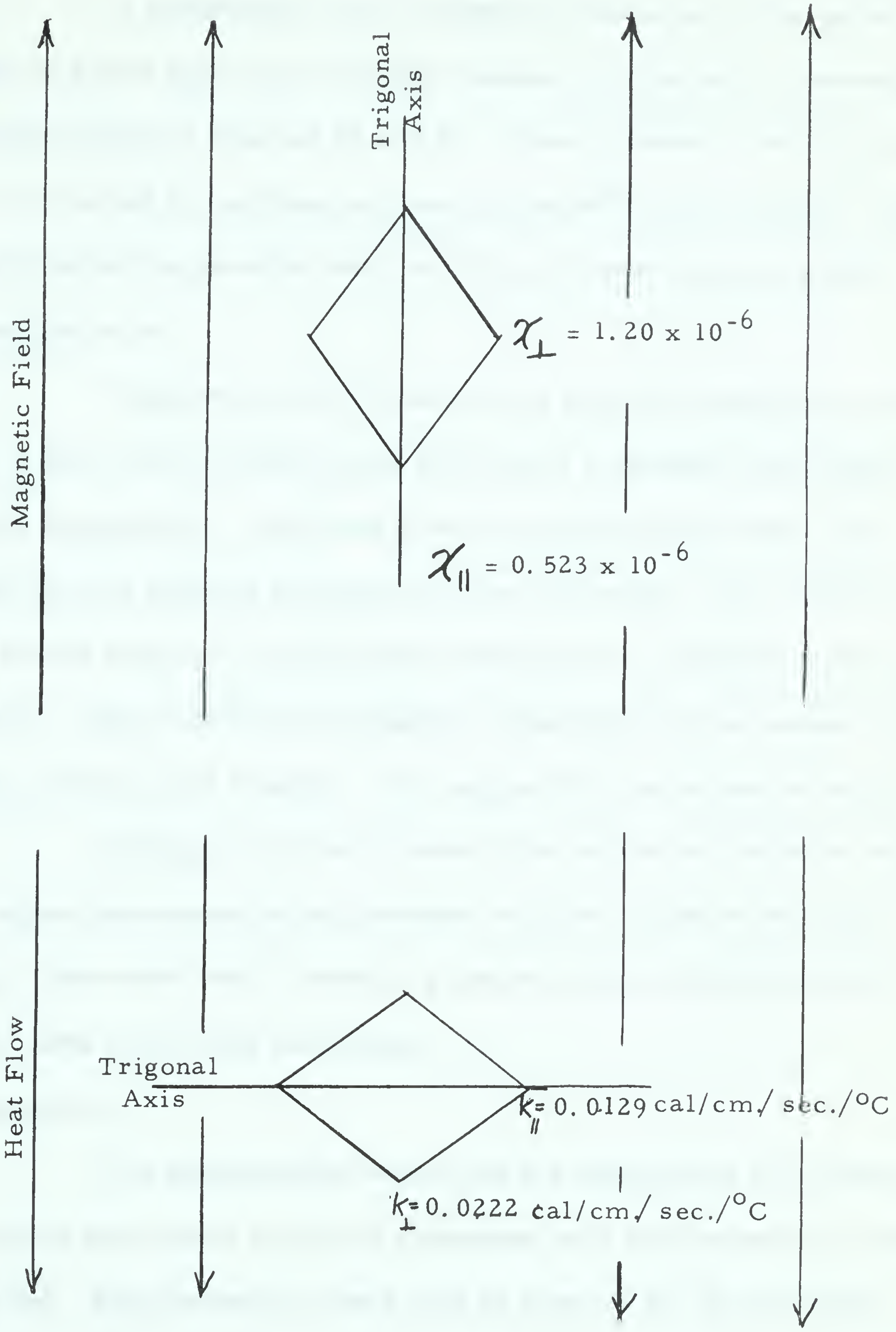
Magnetic Field
Trigonal Axis
$\chi_\perp = 1.20 \times 10^{-6}$
$\chi_\parallel = 0.523 \times 10^{-6}$
Heat Flow
Trigonal Axis
$k_\parallel = 0.0129$ cal/cm./sec./°C
$k_\perp = 0.0222$ cal/cm./sec./°C

Fig. 37. Orientation of a Bismuth Crystal by a Magnetic Field Compared to the Direction of Highest Thermal Conductivity.

A comparison of the preferred orientation of the equiaxial crystals in a field cast ingot with their random orientation in a normally cast ingot is given in Figures 28 and 29. If the crystals in the field cast ingot are oriented in the direction found by Mayr(3) and by Altma(7) the trigonal axis will be parallel with the field and therefore also parallel with the ingot axis.

Figures 26 and 27 compare the dendrite formation at the base of a field cast 85% Bi-Sn ingot with that of a normally cast ingot of the same composition. Dendrites usually grow with the crystal axis oriented so as to produce the best heat flow to the base. For bismuth, this is not the same as the preferred orientation in a magnetic field (see Figure 37). This conflict may be partly responsible for the absence of dendritic growth in the bismuth - rich ingots which were cast in the field.

Mixing of the liquid ahead of the advancing interface would likely reduce the concentration gradients and also decrease the super-cooling. This would tend to produce a larger grain as observed in the equiaxial zone of the field cast ingots.

(2) Segregation

The experimental values for the segregation at the base of the normally cast ingots are not in agreement with the theoretical values (Figure 35). The theoretical curve may be in error for the following reasons:

(a) Inaccurate specific volume data. Thomas and Evans(25) determined the density of bismuth which they had alloyed with very small amounts of tin. They observed a sudden anomalous

rise and fall in the density over the range of composition 98.5% to 100% bismuth. The alloy containing about 98.5% bismuth has the maximum density.

(b) Anomalous values for the solubility of tin in bismuth The range of values is from 2.8% to no solubility (see Goetz and Focke(5)).

The anomalous nature of the data determining the sensitive parameters "a" and "A" places a severe restriction on the reliability of the calculated segregation. The curve shown in Figure 35 is based on the assumption of complete insolubility of tin in bismuth.

The segregation occurring in the ingots cast in the magnetic field is significantly greater than that of the ingots cast normally. It is possible to propose a "field equilibrium diagram" consistent with the observed segregation but it is felt that this would not have any significance until a reason is found for the anomalous results for the normally cast ingots.

SUMMARY AND CONCLUSIONS

(1) For the bismuth-antimony system good agreement was obtained between the segregation values determined by experiment and the segregation values determined by calculation using the equations of the inverse segregation theory.

(2) Solidification in a magnetic field reduced the segregation occurring towards the high bismuth end of the bismuth-antimony system to approximately 40% of its normal value. This may be related to a "field equilibrium diagram" by means of the segregation equations.

(3) For the bismuth-tin system the theoretical and experimental segregation values for the normally cast ingots were not in agreement. Further work is needed to resolve the anomaly.

(4) The magnetic field increased the segregation occuring at the base of the bismuth-tin ingots of high bismuth content by approximately 70% of its normal value.

(5) The crystal morphology of the ingots cast in the field was in all cases somewhat altered from that of the normal ingots, and in the case of the bismuth-tin alloys of high bismuth content a very distinct change occured.

(6) The fundamental mechanisms by which the magnetic field altered the segregation and crystal morphology of the alloys have not yet been established.

BIBLIOGRAPHY

(1) W. Hume-Rothery, "The Structure of Metals and Alloys" The Institute of Metals, London (1945)

(2) R.M. Bozorth, "Ferromagnetism", Von Nostrand, New York (1951)

(3) G. Mayr, Zeits. Natur., A6, 467 (1951)

(4) A. Goetz and A.B. Focke, Phys. Rev., 37, 1044 (1931)

(5) A. Goetz and A.B. Focke, Phys. Rev., 45, 170 (1934)

(6) Y. Shimizu, Sc. Rep. Tohoku Univ., 21, 826 (1932)

(7) A. Altma, Ann. Physik., 32, 489 (1938)

(8) Y. Nakagawa, J. Phys. Soc. Japan, 11, 855 (1956)

(9) W.V. Youdelis, Ph.D. Thesis, McGill University, Montreal (1958)

(10) "Liquid Metals and Solidification" American Society for Metals, Cleveland, Ohio (1958)

(11) C.F. Frank, Disc. Faraday Soc., 5, 48 (1949)

(12) W.K. Burton, N. Cabrera and F.C. Frank, Nature, 163, 398 (1949)

(13) B. Chalmers and U.M. Martius, Phil. Mag., 43, 686 (1952)

(14) B. Chalmers, Proc. Roy. Soc. (London), A 196, 64 (1949)

(15) B. Chalmers, Can. J. Phys., 31, 132 (1953)

(16) W.A. Tiller, J.W. Jackson, J.W. Rutter, B. Chalmers, Acta Metallurgica, 1, 428 (1953)

(17) J.W. Rutter and B. Chalmers, Can. J. Phys., 31, 15 (1953)

(18) R.W. Ruddle, J. Inst. Metals, 77, 1 (1950)

(19) A.J. Cibula, J.Inst.Metals, 76, 321 (1949-50)

(20) D.E. Adams, J.Inst.Metals, 75, 809 (1948-49)

(21) E. Scheil, Z.Metallkunde, 38, 69 (1947)

(22) J.S. Kirkaldy and W.V. Youdelis, AIME Trans., 212, 833 (1958)

(23) W.V. Youdelis and D.R. Colton, AIME Trans., 218, 628 (1960)

(24) A. Wolf and A. Goetz, Phys.Rev., 46, 1095 (1934)

(25) W.R. Thomas and E.J. Evans, Phil.Mag., 17, 65 (1934)

(26) W.A. Tiller and J.W. Rutter, Can.J.Phys., 34, 96 (1956)

(27) C.J. Smithells, Metals Reference Book, Vol II (Butterworth Scientific Publ., London, 1955)

(28) J.M. Daniels, Proc.Phys.Soc. B, 63, 1028 (1950)

(29) J.M. Daniels, Proc.Phys.Soc. B, 66, 921 (1953)

(30) A.L. Underwood, Anal.Chem., 8, 1322 (1954)

(31) J.S. Fritz, Anal.Chem., 12, 1978 (1954)

(32) Kuang Hu Chang, Anal. Chem., 12, 1977 (1954)

(33) E. Pelzel and H. Schneider, Z.Metallkunde, 35, 121 (1943)

(34) "Metals Handbook" - American Society for Metals, Cleveland, Ohio (1948)

(35) T. Takase, J.Inst.Met. Japan, 2, 77 (1938)

(36) G W.C. Kaye, Proc.Roy.Soc. (London) A 170, 561 (1939)

(37) H. Jones, Proc.Roy.Soc. (London) A 135, 537 (1932)

APPENDIX I

CALCULATION OF THE SEGREGATION

The calculations for the maximum segregation as a function of the bismuth content in the bismuth-antimony and bismuth-tin systems were carried out using the equations derived by previous workers(21, 22). A resume of the assumptions made in the derivation, a definition of the symbols and the principal equations follow.

It is assumed that there is complete flow-back of residual liquid during solidification so that no shrinkage porosity occurs. This condition is assured by degassing the melt and by unidirectional solidification. Further, it is assumed that equilibrium conditions exist locally at the solid-liquid interface, and that solid coring is complete while the interdendrite liquid is homogeneous and in equilibrium with the solid at all times. A relatively high rate of diffusion of the solute in the liquid alloy as compared to the solid alloy and a fast solidification rate are the conditions required to validate the latter assumption. The coefficients for self-diffusion of bismuth, antimony and tin are as follows(27):

	Liquid	Solid
Bi	1×10^{-5}(cm^2/sec)	1×10^{-16}
Sb	1×10^{-5}(cm^2/sec)	1×10^{-12}
Sn	1×10^{-5}(cm^2/sec)	1×10^{-9}

Surface exudation, if present, must be corrected for in the segregation determination as it occurs by a different mechanism.

In the segregation calculation an infinitesimal constant volume at the desired point in the solidified ingot is considered and the following notation is used to describe the conditions therein:

C - mean solute concentration at any position in the solidified ingot
c - equilibrium concentration of the solute
m - mass of the solute
v - specific volume
Subscript 's' - liquidus (from the German word schmelz)
Subscript 'k' - solidus (from the German word krystal)
Subscript 'E' - refers to conditions present when the eutectic temperature is reached

The maximum segregation at any point in the solidified ingot is given by:

$$\Delta c = C - c_o = \frac{\dfrac{m_{sE}c_{sE}}{a_E} + m_{kE}C_{kE}}{\dfrac{m_{sE}}{a_E} + m_{kE}} - c_o$$

where

c_o - the initial liquid concentration in the liquid which is assumed uniform
a - the contraction coefficient

$$a = \frac{v_k}{v_s} + \frac{c_s - c_k}{v_s} \quad \frac{dv_s}{dc_s}$$

and reduces to

$$a = \frac{v_{kE}}{v_{sE}} \quad \text{for the eutectic liquid}$$

The basic differential equation for the calculation of the mass terms in (1) is

$$\frac{dm_s}{m_s} = -a\,\frac{dc_s}{Ac_s} \qquad (3)$$

where "A" is defined by

$$A = \frac{c_s - c_k}{c_s}$$

In both the bismuth-tin and the bismuth-antimony systems the concentrations of the solute in the liquid and solid masses at equilibrium in the sample volume, c_s and c_k respectively, and the corresponding specific volumes, v_s and v_k, are non-linear functions of the bismuth concentration necessitating a step-wise integration for the solution of (3). Equation (3) has been solved by Scheil$^{(21)}$ and by Kirkaldy and Youdelis$^{(22)}$ to obtain the various mass terms in the segregation equation (1).

The mass term for the cored crystals is given by

$$m_{k_{i+1}} = m_{k_i} + \frac{m_{s_i} - m_{s_{i+1}}}{a_i} \qquad (4)$$

and for the liquid by

$$m_{s_{i+1}} = m_{s_i}\left(\frac{c_{s_{i+1}}}{c_{s_i}}\right)^{-a_i/A_i} \qquad (5)$$

The solute content in the cored primary crystals is given by

$$m_{k_{i+1}}\,c_{k_{i+1}} = m_{k_i}c_{k_i} + \left(\frac{1 - A_i}{A_i - a_i}\right)\left(m_{s_i}\,c_{s_i}\right)\left[\left(\frac{c_{s_{i+1}}}{c_{s_i}}\right)^{\frac{A_i - a_i}{A_i}} - 1\right] \qquad (6)$$

The summation of the terms in equations (4) (5) and (6) is taken to the eutectic temperature to obtain the terms m_{sE}, m_{kE} and

$m_{kE}c_{kE}$. The values which resulted from the calculation for the maximum segregation are plotted in Figure 34 for the bismuth-antimony system and Figure 35 for the bismuth-tin system for comparison with experimental results.

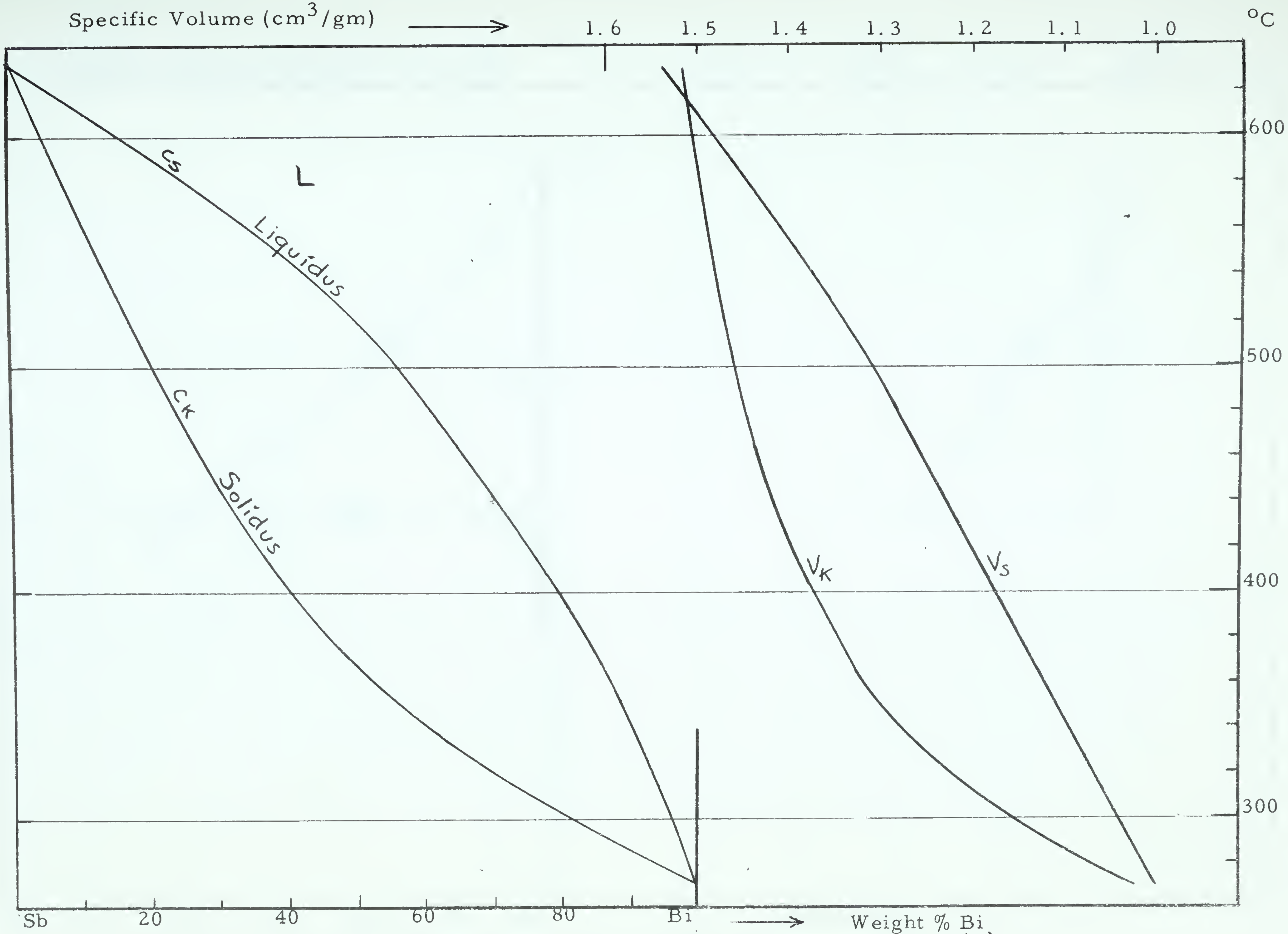

Fig. 38 Equilibrium Diagram and Specific Volume Data for the System Bi-Sb.(33)

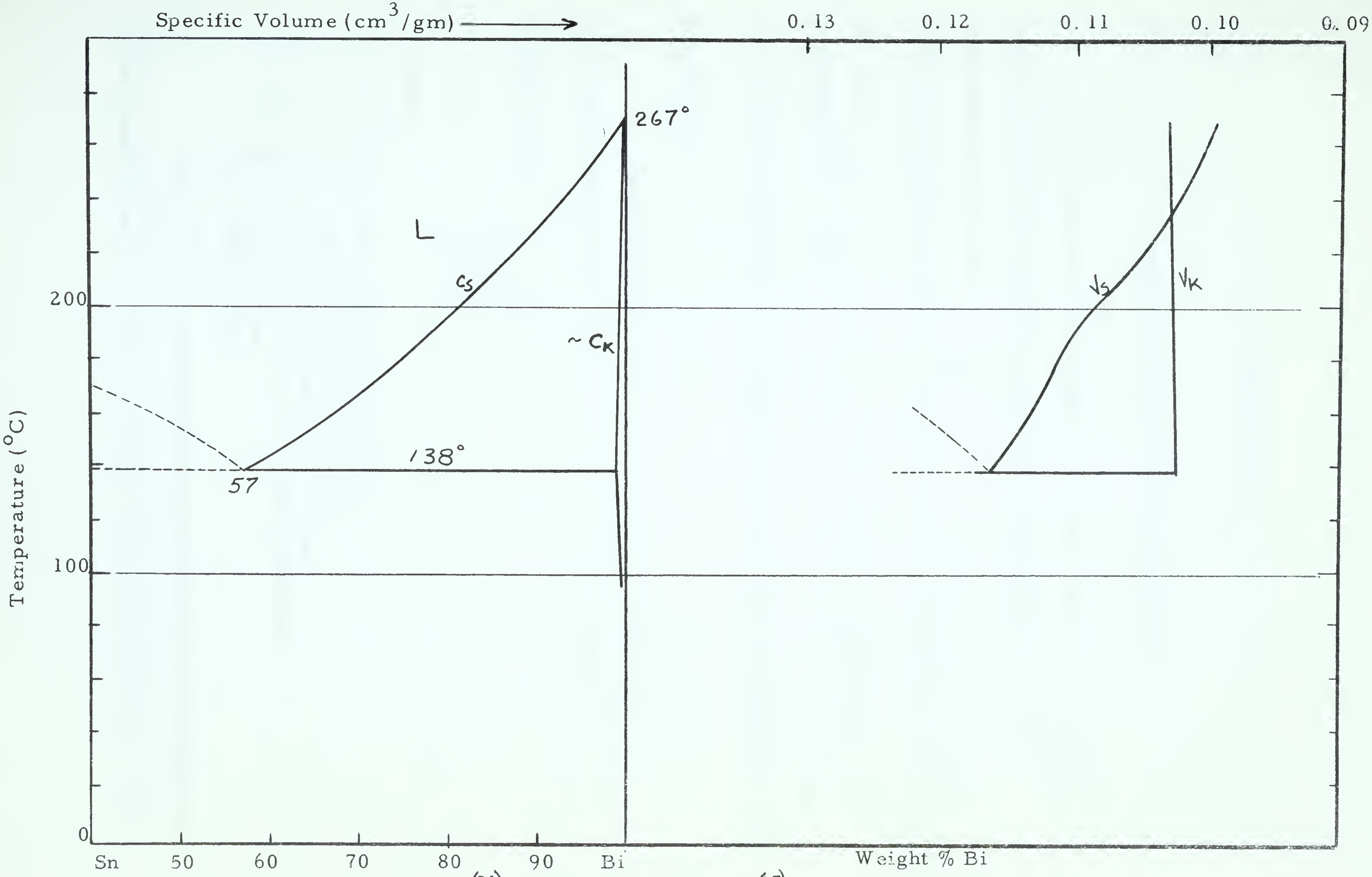

Fig. 39 Equilibrium Diagram(34) and Specific Volume Data(35) for the System Bi-Sn

APPENDIX II

CONSTRUCTION OF THE SOLENOID

It was desired to produce a magnetic field of ten kilogauss uniform to within a few percent over a working volume one inch in diameter and two inches in length. After a literature search, a water cooled solenoid was selected as the best type of instrument for this purpose due to its relatively low cost, ease of construction, compatibility with available power supplies, and accessible working volume. The design which is described below was adapted from that used by Daniels.(28, 29)

Theoretical

The field at the center of a coil with a winding space of rectangular cross section has been shown (Cockroft, 1928) to be given by the formula:

$$H = G\left(\frac{W\eta}{a\rho}\right)^{1/2}$$

where

H = the field strength (gauss)
W = the power dissipated (watts)
a = the inner radius of the coil (cm)
ρ = the resistivity of the winding material
G = shape factor
η = filling factor

To attain low pressure and temperature gradients within the coil successful practice calls for a value for the filling factor η in the

range 0.5 - 0.7. As demonstrated by Daniels, a field uniform to within three percent may be produced over a working cylindrical volume of axial length twice the diameter by a coil of outer radius 3a, axial length 6a and with a space of 0.25a omitted from the center. For such a coil the shape factor $G = 0.159$.

Calculation

The dimensions of the copper strip were calculated as follows:

Total volume of winding space

$$V = \pi \ell (32)^2 - \pi \ell (a)^2 \qquad \text{Where} \quad \ell = 6a$$
$$= 500 \text{ cm}^3$$

Volume of copper required

$$\eta V = 300 \text{cm}^3$$

The resistance of the coil

$$R = \frac{(\text{voltage of the power source})^2}{\text{total power used}}$$
$$= 0.05 \text{ ohms}$$

The cross sectional area "A", and the length "L" of the copper strip then follow by combining the above relations

$$R = \rho \frac{L}{A} \quad \text{and} \quad V = LA$$

which gave the values

$$A - 0.01639 \text{ in.}^2$$
$$L = 96 \text{ feet}$$

The core was divided into eight pancake coils for convenience in making

the connectors. Allowance for insulation between the successive coils then fixed the value for the cross section of the copper strip at 0.375 x 0.044 inches.

The rate of flow of the cooling water was arrived at by dividing the total power to be dissipated by an assumed temperature rise and efficiency factor. The result was 20 gpm.

Details of Construction

The central tube of the solenoid was cut from a length of hard brass tubing of one inch inside diameter and 0.0625 inch wall thickness. The section over which the coils were to be mounted was insulated with a layer of polyethylene which was 0.0625 of an inch thick. This was applied by wrapping the tube with layers of polyethylene film which were bonded to the tube and to each other by warming in an oven.

The eight pancake coils were wound in pairs around brass sleeves 0.040 inches in thickness, which were prepared to be a press fit over the insulated portion of the central tube. The pancake coils were formed as follows:

The copper strip was cut into four pieces each of which was 24 feet in length. The strips were then insulated by applying a winding of 0.010 inch diameter nylon monofilament at a spacing of twelve turns per inch. This was accomplished by pulling the strip through the hollow spindle of the lathe, using a clamp attached to the total carriage, while

a winder rotated by chuck applied the nylon monofilament. The winder consisted of a bobbin, guides of thin steel wire, and a tension device from a sewing machine all mounted upon a short length of three inch diameter brass pipe.

Each insulated piece of copper strip was wound around a brass sleeve into two continuous pancake coils. The center turn was stabilized with wedges of acrylic plastic and the coils were insulated from one another by a spider cut from 0.040 inch melamine plastic sheet. These insulators had an outer rim extending to the walls of the casing to prevent the cooling water from flowing around the coils.

The pairs of coils, with insulating spiders between them, were slipped over the central tube and connected together by silver soldering copper bars between the ends. The assembled coils were then wrapped with a layer of plastic screening and clamped by bolting strips of 0.0625 inch brass around them. The copper terminals were soldered onto each end to complete the solenoid core assembly.

The solenoid casing consisted of a cylinder formed from 0.125 inch brass fitted with end pieces of one inch acrylic plastic. O-ring seals were used at the ends of the cylinder and on the terminals and tubes extending through the end pieces.

The cooling water entered through two one-half inch inlets in the bottom of the solenoid, passed through the core and out through two similar outlets at the top. The heat was removed from the cooling

water by passing it through sixty feet of one inch copper pipe immersed in flowing tap water. The water was circulated by means of a one inch gear pump driven by a 3/4 H. P. motor.

The solenoid mounting, connections and controls are illustrated in the photograph of the apparatus (Figure 4) and in the schematic sketch (Figure 4)).

Solenoid Operation

The theoretical formula for the calculation of the field produced was previously given as

$$H - G\left(\frac{W\eta}{a\rho}\right)^{1/2}$$

Using the values for this solenoid

$G = 0.159$
$W = 25,000$ watts
$\eta = 0.60$
$\rho = 1.72 \times 10^{-6}$ ohm cm
$a = 1.50$ cm

The value for the field produced is theoretically established at

$H = 12,200$ gauss

The measured value for that power consumption was 13,000 gauss. The higher value is thought to be due to a slightly better filling factor and smaller value for the inner radius "a".

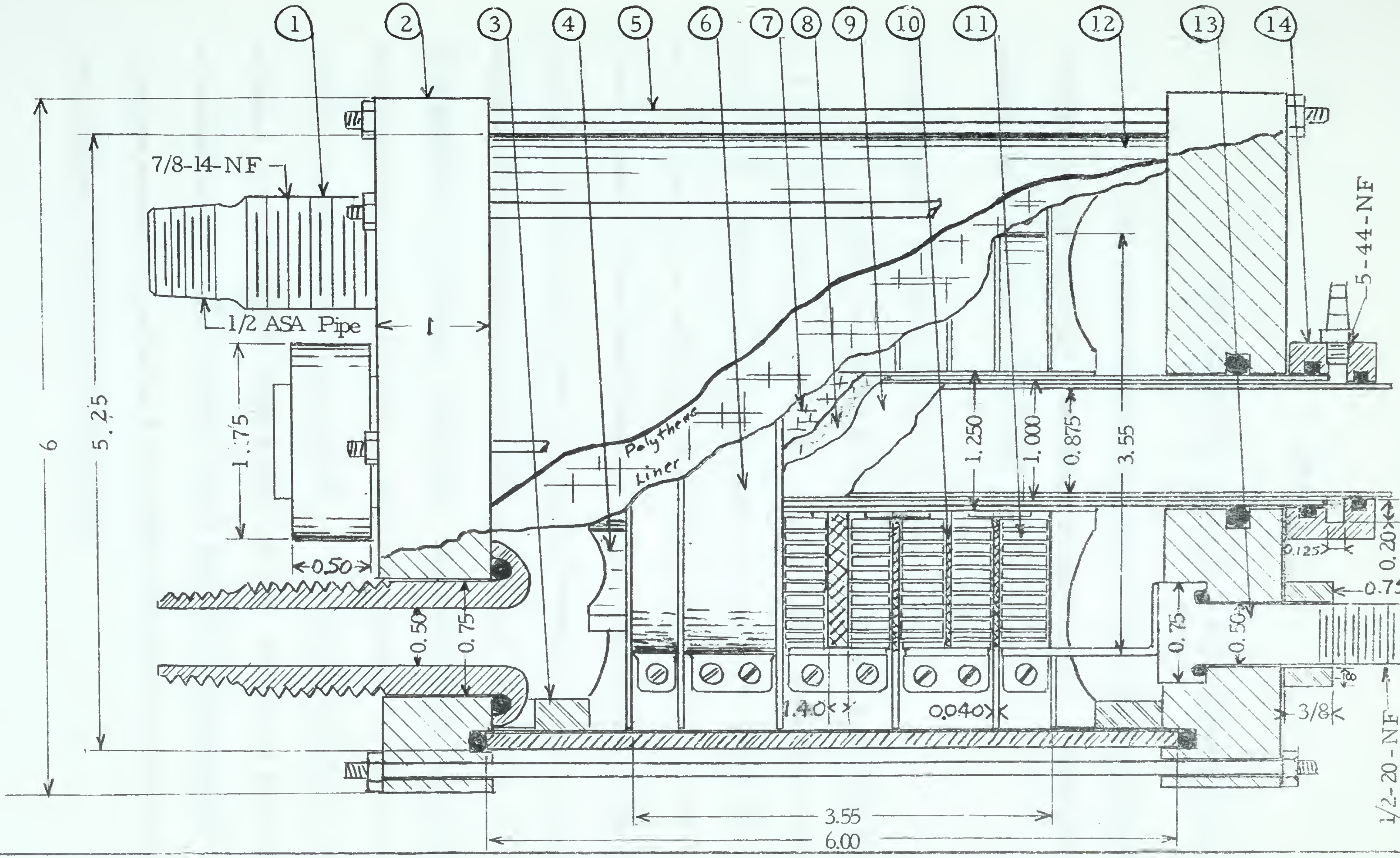

1. Water Inlet
2. End Pieces (Plastic)
3. Spacer
4. Press. Plate
5. Tie Rod
6. Band
7. Insulation (Polythene)
8. Central Tube
9. Inner Tube
10. Insulator (Melamine)
11. Copper Strip
12. Case
13. Power Terminal (Copper)
14. Water Jacket End Piece

Fig. 40 - Cross Section of the Solenoid. All parts are of brass unless otherwise noted. The end pieces have been rotated 90° relative to each other for convenience in showing the construction.

APPENDIX III

METHODS OF ANALYSIS FOR BISMUTH (30, 31, 32)

The methods used are based on the selective titration of the strongly yellow collored bismuth-thiourea complex with EDTA under conditions of carefully controlled pH.

Procedure for Bismuth-Antimony Alloys

Weigh in a finely granulated sample of the alloy and place in a 250 ml. beaker. Add 10 ml. of aqua regia and allow to dissolve in the cold. Add 2.5 grams tartrate salt, dilute to about 50 ml. and stir to dissolve the tartrate. Make the solution up to an exact volume in a volumetric flask with distilled water. The aliquots pipetted from the flask should contain about 50 mg. of bismuth. To each aliquot add a slight excess of 0.01 MEDTA by means of a burette. (1 ml. of 0.01 MEDTA = 2.090 mg. bismuth). Add 0.01 grams thiourea per ml. of solution and stir to dissolve. Add dilute ammonia, dropwise with constant stirring, until the solution is colorless. Warm for a few minutes in a water bath, then adjust the pH. with more dilute ammonia to a value of 1.5. Back titrate with 0.005 M bismuth solution. This titration should be performed soon after the pH is raised to avoid the precipitation of hydrolysis compounds.

Procedure for Bismuth-Tin Alloys

Weigh in a finely granulated sample of the alloy containing about 200 mg. of bismuth and place in a 150 ml. of a mixture containing eight parts HBr to two parts Br_2. Allow to dissolve in the cold, then add 15 ml. of perchloric acid and heat until copious white fumes appear and the solution turns colorless. The appearance here of a finely divided white precipitate is normal. Cool, dilute to a convenient volume with distilled water acidified to a pH less than one with nitric acid and swirl to dissolve the precipitate. Then adjust to an exact volume in a volumetric flask. The remainder of the procedure is the same as that given for the titration of bismuth-antimony alloys.

Determination of Errors

The root mean square error occurring in the control sample determinations was $\pm 0.03\%$. Two such errors are combined in a segregation determination giving a probable error in the experimental segregation values of $< \pm 0.10\%$.

B29787